INSTITUTE OF PHYSICS PUBLISHING JOURNAL OF PHYSICS D: APPLIED PHYSICS

J. Phys. D: Appl. Phys. **39** (2006) R439–R459 doi:10.1088/0022-3727/39/22/R02

TOPICAL REVIEW

Cluster beam deposition: a tool for nanoscale science and technology

K Wegner[1,2], P Piseri[3], H Vahedi Tafreshi[4] and P Milani[3,5]

[1] Tethis S.r.l., Via Russoli 3, 20151 Milano, Italy
[2] Particle Technology Laboratory, Institute of Process Engineering, Department of Mechanical and Process Engineering, ETH Zurich, CH-8092 Zurich, Switzerland
[3] CIMAINA and Dipartimento di Fisica, Università di Milano, Via Celoria 16, 20133 Milano, Italy
[4] NCRC, North Carolina State University, 2401 Research Dr., Raleigh, NC 27695-8301, USA

E-mail: pmilani@mi.infn.it

Received 21 June 2006, in final form 7 August 2006
Published 3 November 2006
Online at stacks.iop.org/JPhysD/39/R439

Abstract
Gas phase nanoparticle production, manipulation and deposition is of primary importance for the synthesis of nanostructured materials and for the development of industrial processes based on nanotechnology. In this review we present and discuss this approach, introducing cluster sources, nanoparticle formation and growth mechanisms and the use of aerodynamic focusing methods that are coupled with supersonic expansions to obtain high intensity cluster beams with a control on nanoparticle mass and spatial distribution. The implication of this technique for the synthesis of nanostructured materials is also presented and applications are highlighted.

(Some figures in this article are in colour only in the electronic version)

1. Introduction

The presence of nanoparticles in industrial processes dates back well before the advent of nanotechnology [1, 2]: carbon nanoparticles as rubber additives for tyres [3] or titania nanoparticles for pigmentary applications [4, 5] represent a paradigm of mass production of nanoscale objects. In the last decade, the increasing understanding and control of the fundamental properties of nanoparticles has stimulated the interest in their use as building blocks of devices and systems with sophisticated properties and functionalities [6]. The ultimate goal of the nanotechnological approach is to provide new paradigms of production; however, it is reasonable to consider that the success of nanotechnology will rely on its capability of complementing actual technologies before substituting them [7].

The success of manufacturing approaches based on the assembling of nanoparticles is largely determined by the established infrastructure and customer base with cost reduction as a general benchmark. Other important parameters are for instance, the possibility of improvement in performance per unit cost and the compatibility with other production technologies (for example, in the semiconductor industry) [8].

The design and production of devices containing nanoparticles and nanomaterials require the capability of integrating different components at different length scales in terms of structure, chemical composition, packaging, etc. It is thus necessary to determine the structure and chemical status of nanoparticles and to transfer them onto suitable substrates or into matrices with a very precise control on positioning in an exactly defined area. Once deposited in a device, the nanoparticles should retain their properties and individuality.

A crucial point to be solved for a real technological breakthrough is the possibility of manipulating nanoscale objects [9]. The general term 'manipulation' is used here with special reference to the following meanings: (i) the ability to sort the objects in terms of a size or geometry classification; (ii) the ability to control the position and (iii) the ability to modify them physically or chemically. As most of the available nanoparticle synthetic routes are not able to produce

[5] Author to whom any correspondence should be addressed.

a perfectly monodisperse population, a refinement of the particle population is often necessary depending on the specific application. The second and third requisites are naturally connected to the fabrication of a class of systems exploiting the extraordinary properties of the nanoscale objects.

Among different processes for the production of nanoparticles, gas-phase routes are very popular both for large scale production and for fundamental studies [2]. A number of extraordinary qualities make the gas-phase approach a very interesting technique for the fabrication of nanostructured systems. Gas-phase synthesis is an established and well-developed process able to produce large scale quantities of nanoparticles [10–12] with a high level of control on particle physico-chemical properties such as phase and composition [13]. Effective post-synthesis treatment such as high temperature annealing [14, 15] and coating [16] has been demonstrated, as well as the compatibility of aerosol methods with the high purity standards of the semiconductor industry [17]. Positioning of gas phase particles on a surface with a resolution in the 100 nm range and below has been shown [18] as well as the possibility of micropatterning particle-assembled thin films [19].

Among different gas phase approaches to nanofabrication, the deposition of clusters from supersonic beams is gaining increasing attention extending the interest for this field from basic to applied research [20]. Aggregates ranging from a few atoms to a few thousands of atoms, known as clusters, are produced and carried in supersonic expansions and have been the playground for the characterization of the transition from atomic behaviour to solid-state collective features. The role of the electronic structure and of the lattice structure in determining the stability of the clusters has been recognized since 30 years and has been widely studied [21]. However, the spectroscopic characterization of isolated clusters remains the holy grail for scientists since the high dilution of the vast majority of clusters prevents the use of standard physico-chemical characterization techniques.

Cluster beam deposition (CBD) has great potential for the production of nanostructured and nanocomposite films although several technical limitations have hampered its use as one of the bottom-up approaches to the synthesis of nanomaterials [20]. Supersonic expansions have several advantages for cluster manipulation over effusive beams that make this approach very powerful for the deposition of nanostructured films and the coupling with microfabrication techniques. This is due to the fact that supersonic CBD favours the manipulation and positioning of nanoparticles by the exploitation of nanoparticle inertial properties [22, 23].

Many theoretical and experimental approaches have been developed to solve the problem of neutral nanoparticle manipulation in the gas phase [24]. The merging of solutions and models developed for aerosols and for supersonic expansions has stimulated a novel and interdisciplinary route to this problem [24, 25]. The solutions proposed and tested in these last years have shown that the synthesis of nanostructured materials with tailored structural and functional properties can be obtained by exploiting aerodynamical focusing in seeded supersonic beams. In particular the use of aerodynamic lenses [26,27] allows an unprecedented control on nanoparticle spatial and mass distribution, while keeping very high fluxes and deposition rates [24]. A further improvement in aerodynamic manipulation techniques for different gas phase synthesis methods is opening new perspectives for the integration of gas phase nanoparticle production into the large and well-consolidated arena of physical vapour deposition technologies [23].

In this review we will present and discuss features of gas-phase cluster production and deposition relevant for the fabrication of nanostructured systems. In particular, we will concentrate on those fundamental aspects affecting the performance of different gas phase production and manipulation methods with their advantages and bottlenecks in view of possible technological uses. After this introduction, section 2 is devoted to the basic principles of nanoparticle formation and growth in the gas phase, while section 3 describes methods for manipulation and handling of free nanoparticles. Cluster sources are described in section 4; section 5 discusses patterning and coupling to planar technologies. An overview of applications and conclusions are given in sections 6 and 7, respectively.

2. Gas phase nanoparticle formation and growth

Formation and growth processes of objects relevant for CBD follow the same physical and chemical mechanisms as any gas-phase particle synthesis process. These mechanisms have been extensively studied in aerosol synthesis, the gas-phase manufacture of nanoparticles at atmospheric pressure [28], and can also be applied to the cluster sources used in CBD processes.

In gas phase synthesis, nanoparticles are made by 'building' them from individual atoms or molecules up to the desired size. Cluster embryos are formed either by physical means such as condensation of a supersaturated vapour or by chemical reaction of gaseous precursors. Examples include inert gas condensation [29, 30], plasma [31] and flame processes [32]. Depending on the embryo concentration, system temperature and pressure, these clusters continue to grow to larger entities by coagulation and coalescence and/or surface growth. Particle dynamics [33, 34] aim at a mathematical description of these growth processes, taking the entire nanoparticle population into account.

2.1. *Particle formation*

Formation of particles in the gas phase takes place either by homogeneous nucleation or by coagulation (collision) processes. The starting material can be vaporized from a hot source into a low density inert gas employing Joule heating, thermal plasma or laser ablation. Cooling of the vapour rapidly leads to supersaturation followed by homogeneous nucleation and the formation of first product clusters [35].

Often, a chemical reaction is the first step in the nanoparticle formation process. This is the case when the background gas in the evaporation process is not inert but reacts with the precursor vapour to form product molecules, for instance, in the synthesis of aluminium nitride by the reaction of aluminium vapour with ammonia in an aerosol flow reactor [36]. Another prominent and the industrially most relevant example of gas-phase particle formation involving

chemical reactions is the introduction of a volatile precursor such as a chloride or organometallic compound into a high temperature environment, for instance, a flame [1, 33]. Here, precursor decomposition, oxidation, hydrolysis or, depending on the environment, any other reaction lead to the formation of product molecules.

The thermodynamics of the system determine whether these product molecules grow to clusters by homogeneous nucleation or by coagulation. A criterion to determine the formation path of a cluster is its thermodynamically critical diameter, the Kelvin diameter $d_{1,C}$:

$$d_{1,C} = \frac{4\gamma V_{\mathrm{mol},1}}{k_B T \ln(S)}. \tag{1}$$

Here, γ and $V_{\mathrm{mol},1}$ are the surface tension and the molecular volume of the cluster, S is the dimensionless saturation ratio at temperature T and k_B is the Boltzmann constant. A nucleus is stable when its critical diameter is much smaller than the diameter of a single molecule of the product species. In this case, there will be no growth or shrinkage by condensation or evaporation and the particle will form by coagulation [37]. In the case of unstable clusters, particles are formed by homogeneous nucleation: balanced condensation and evaporation of molecules to and from clusters of the product species. The Gibbs–Kelvin equation (1) should be used with caution, though, as it relies on macroscopic particle properties like surface tension. For ceramics, the critical cluster diameter is typically smaller than the molecular diameter and particle formation takes place by coagulation. Metal nanoparticles on the other hand are usually formed by homogeneous nucleation, for instance, in the production of iron nanoparticles in a plasma reactor [31] or the synthesis of bismuth nanoparticles by evaporation–condensation [38].

2.2. Particle growth

The newly formed particles continue to grow either by surface growth (addition of atoms or molecules to the particle) or by coagulation (inelastic particle–particle collisions) which is usually followed by coalescence.

Coagulation describes particle–particle collisions due to Brownian motion or other mechanisms such as shear or electrostatic forces. Typically, it is applied to particle growth in combination with coalescence. For the description of particle growth by coagulation, one has to distinguish between collisions in the free molecular regime (particle diameter d_p smaller than the mean free path of the gas λ) and in the continuum regime ($d_\mathrm{P} \gg \lambda$). Neglecting the particle morphology and the spread of the particle size distribution, the classical theory for Brownian coagulation of monodisperse spheres in the continuum regime at temperature T is used to calculate d_p [28]:

$$d_\mathrm{P} = d_{\mathrm{P},0}\left(1 + \frac{4k_B T N_0}{3\mu} t\right)^{1/3}, \tag{2}$$

where $d_{\mathrm{P},0}$ and N_0 are the initial particle diameter and concentration, respectively, μ is the dynamic viscosity of the gas and t is the residence time. If the particle diameter is much smaller than the mean free path of the gas, as is usually the case with clusters, the coagulation theory in the free molecular regime has to be applied. Neglecting again the spread of the particle distribution and the morphology:

$$d_\mathrm{P}^{5/2} = d_{\mathrm{P},0}^{5/2} + \frac{10}{\pi}\left(\frac{6k_B T}{\rho_\mathrm{P}}\right)^{1/2} V_\mathrm{vol} t, \tag{3}$$

where V_vol is the total volume of particles per unit volume of gas and ρ_P is the density of the particles.

Particles that grow by Brownian coagulation typically reach asymptotic distributions, the so-called self-preserving size distributions [28]. These distributions remain invariable with time when the particle size and concentration are scaled with the average particle volume. For an initially monodisperse aerosol, it takes time t_SPSD to reach the self-preserving size distribution. In the free molecular regime, t_SPSD is [39]:

$$t_\mathrm{SPSD} = \frac{4}{\left(\frac{6k_B T}{\rho_P}\right)^{1/2} N_0^{5/6} \left(\frac{3V_\mathrm{vol}}{4\pi}\right)^{1/6}}. \tag{4}$$

The geometric standard deviation for the number self preserving size distribution is about 1.46 while that for the mass is about 1.3 [39, 40]. These asymptotic distributions place a lower limit on the reduction of the polydispersity of particles grown by coagulation.

If the entire particle size distribution rather than a monodisperse aerosol is to be considered for particle growth by coagulation, the population balance equation in the free molecular and continuum regimes has to solved using computer codes.

It should be noted that the particle morphology may affect the rate of particle growth by coagulation. In the free molecular limit, agglomerates collide much faster than spheres of the same mass since they have more surface area for collisions. In the continuum limit, the enhanced collision surface of agglomerates does not play a major role because agglomerates experience enhanced drag by the medium.

Surface growth consists of a first step of molecule or atom transport to the surface of an already-formed particle and a second step involving a chemical reaction or a phase change at the particle surface. Especially during the first stages of particle formation from supersaturated vapour, surface growth can be significant as the initially formed clusters act as condensation seeds for the remaining vapour. By controlling the supersaturation at a low level, particle nucleation can be slowed down while the rate of surface growth by vapour deposition can be increased [34]. In systems with chemical reaction, species transported to the particle surface either react with the particle thus changing its chemistry or react at the particle surface with other gaseous species with the reaction product being deposited on the surface. Surface growth can contribute to the entire particle growth process in systems where vapour or gas molecules are present in sufficient quantity. In general, the rate of change of the particle diameter d_p at temperature T by vapour deposition in the free molecular regime is given by [28]:

$$\frac{\mathrm{d}d_\mathrm{P}}{\mathrm{d}t} = \frac{2v_1(p_1 - p_\mathrm{d})}{(2\pi m k_B T)^{1/2}} F_1, \tag{5}$$

where v_1 is the volume of the transported molecule in the particle phase, p_1 is the partial pressure of the gas or vapour

far from the particle and p_d is the partial pressure at the particle surface obtained from the equilibrium vapour pressure over a flat surface using the Kelvin equation (1). F_1 is the Fuchs–Sutugin factor for bridging the free molecular with the continuum regime [41]. In the continuum regime, the rate of change of the particle diameter is [28]:

$$\frac{\mathrm{d}d_P}{\mathrm{d}t} = \frac{4Dv_1(p_1 - p_d)}{d_P k_B T} F_2, \tag{6}$$

where D is the diffusion coefficient of the gas or vapour and F_2 is the Fuchs–Sutugin factor for bridging the continuum with the free molecular regime.

If the nucleation burst produces particles from size d_0 to $d_0 + \Delta d$, the upper and lower bound sizes will increase due to vapour deposition but the size range will not change. Thus, the relative range of particle sizes $\Delta d/d$, will decrease as the particles grow, leading to a narrower distribution than that obtained by growth through coagulation, as observed by Okuyama *et al* [42]. This has been used for instance by Bowles *et al* [43] who generated clusters of controlled size and then grew them by vapour deposition, leading to a very narrow particle size distribution.

The classical coagulation theory assumes rapid and full coalescence of particles after a collision event, resulting in spherical product particles. Full coalescence, however, only takes place at sufficiently high temperature at which particles are present as low viscosity liquid droplets. At lower temperature, the two or more colliding particles will stick to each other and fuse by sintering, often resulting in agglomerates rather than spherical product nanoparticles. Thus, a sintering rate has to be introduced into the description of particle growth. The sintering kinetics depend strongly not only on material and temperature but also on particle size. Driven by surface energy minimization, coalescence or sintering of two particles can occur via viscous flow or solid state diffusion mechanisms. Typically, however, the application of macroscopic material properties to nanoparticles does not describe the observed coalescence or sintering rates. The significantly different thermodynamic properties of nanoparticles with diameters below about 10 nm that are for instance evident from the melting point decrease of gold nanoparticles with decreasing particle size [44] can result in large errors in the predicted coalescence rate [45]. Thus, models must be applied to more accurately describe the observed coalescence rates of nanoparticles [46, 47].

2.3. The population balance equation

The particle formation and growth processes described in the previous paragraphs usually take place simultaneously. Depending on the system investigated, additional effects such as electrical charges or intraparticle chemical conversion might play a role in the particle growth process. Furthermore, in an accurate mathematical description the entire polydisperse particle population should be considered rather than an idealized monodisperse aerosol. The general mathematical description for the evolution of a particle size distribution in time and space is by a population balance equation:

$$\begin{aligned}\frac{\partial n(v)}{\partial t} = &\underbrace{-\nabla n\vec{u}}_{\text{(a)}} + \underbrace{\nabla D \nabla n}_{\text{(b)}} + \underbrace{\frac{\partial}{\partial v}\left(n\frac{\mathrm{d}v}{\mathrm{d}t}\right)}_{\text{(c)}} - \underbrace{\nabla \vec{c} n}_{\text{(d)}} \\ &+ \underbrace{\frac{1}{2}\int_0^v \beta(\tilde{v}, v-\tilde{v}) n(\tilde{v}) n(v-\tilde{v})\,\mathrm{d}\tilde{v}}_{\text{(e)}} \\ &- \underbrace{\int_0^\infty \beta(v, \tilde{v}) n(v) n(\tilde{v})\,\mathrm{d}\tilde{v}}_{\text{(e)}} \\ &- \underbrace{S(v)n(v) + \int_v^\infty \gamma(v, \tilde{v}) S n(\tilde{v})\,\mathrm{d}\tilde{v}}_{\text{(f)}}\end{aligned} \tag{7}$$

In this general example of a population balance, the variation of the particle size distribution function n with time t is influenced by convection (a), diffusion (b), surface growth (c), external forces (d), coagulation (e) and fragmentation (f). Thereby, u is the velocity, D the diffusion coefficient, v the particle volume, c the particle velocity, β the collision function, S the rate of fragmentation and γ the fragment size distribution (see Friedlander [28]). The collision function β describes coagulation due to Brownian motion, shear or electrical charges. Furthermore, particle morphology, expressed for instance by the fractal dimension, as well as information on coagulation in the free molecular, continuum or transition regime are considered in the collision function. The form of the population balance and its terms have to be adopted to the physically relevant growth processes of the investigated system. Several examples are given by Friedlander [28].

As the population balance equation is a nonlinear, partial integrodifferential equation, numerical solutions are usually required. A discrete solution accounting for all particle sizes leads to more than 10^9 differential equations to be solved simultaneously if the entire growth spectrum below 1 μm is considered [48]. Therefore, the solution of the discrete population balance is usually only carried out for a limited size fraction, describing for instance the early stages of growth. Computationally less intensive but also less accurate are moment, sectional or monodisperse models that rely on simplifying assumptions. Moment models make assumptions regarding the shape of the particle size distribution [49], sectional models divide the size distribution into size classes and sections, which are characterized by a mean value of a particle characteristic [50] while monodispersity can be considered for rough estimates.

2.4. Control of particle synthesis

Depending on the governing growth mechanisms and process conditions, product nanoparticles are individual, dense particles or fractal-like agglomerates consisting of at least two subunits, the so-called 'primary particles'. Depending on the strength and nature of the bonds connecting the primary particles, an agglomerate is termed hard or soft [34]. In hard agglomerates, primary particles are strongly bound together as a result of sintering necks while in soft agglomerates the interparticle bonds are of physical nature and in most cases van der Waals forces. Soft agglomerates are formed at temperatures too low for significant coalescence and unlike hard agglomerates they may be separated into their component primary

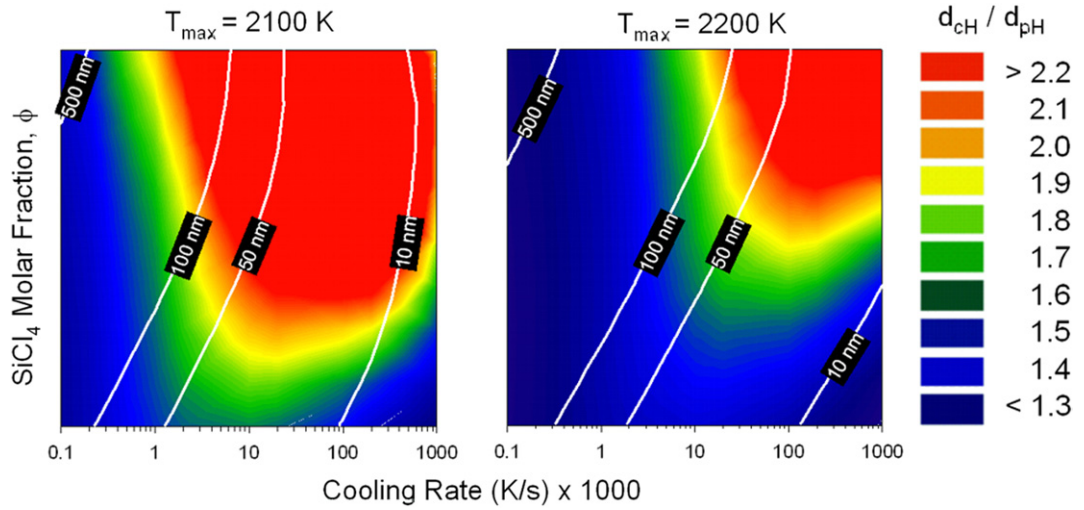

Figure 1. Mapping the degree of silica nanoparticle agglomeration in flame aerosol reactors expressed as the ratio of the collision diameter of the hard agglomerate and the primary particle diameter (d_{cH}/d_{pH}) in the process parameter space of the inlet $SiCl_4$-precursor molar fraction (ϕ) and the cooling rate for reactor residence times of 2 ms at 2100 and 2200 K maximum process temperature (T_{max}). Isopleths of the primary particle diameters (d_{pH}'s, nm) are shown also (white lines). Increasing T_{max} reduces the degree of agglomeration and increases the primary particle diameter. Pictures reproduced with permission from Langmuir 2004 **20** 5933–9 [51]. ©2004, American Chemical Society.

particles with relative ease. The temperature field, reactor residence time and chemical additives affect the particle size and the extent of agglomeration and, consequently, the particle morphology. If the growth conditions are such that the rate of coalescence is faster than that of coagulation, spherical particles are obtained. However, as particles grow, the sintering rate decreases due to increasing particle size and typically due to decreasing reactor temperature so that particle coalescence usually becomes slower than coagulation. As a result, irregularly shaped agglomerate particles are formed [32].

Especially in ceramic nanoparticle production full coalescence is only observed at very high temperatures. Accounting for simultaneous gas phase chemical reaction, coagulation, and sintering during the formation and growth of silica (SiO_2) nanoparticles, Tsantilis and Pratsinis [51] computed maps showing the degree of agglomeration as a function of the reactor temperature, precursor concentration and cooling rate. Figure 1 shows how an increased process temperature and high cooling rates of 10^5 to 10^6 K s^{-1} can avoid the formation of hard agglomerates even at rather high concentrations. This was observed experimentally by Wegner *et al* [52] for titania nanoparticles when rapidly quenching a synthesis flame by expansion through a critical flow nozzle.

3. Manipulation and handling in the gas phase

As outlined in the previous section, gas phase synthesis usually does not give monodisperse particles but a size distribution, the width of which mainly depends on the synthesis conditions in the particle source. For many applications, however, a refinement of the particle population is desired. The ability to sort nanoparticles in the gas phase directly after their synthesis in terms of a size or geometry thus is of major importance. For device fabrication involving controlled particle deposition on substrates, a second requisite is of importance: the ability to deposit nanoparticles with very high lateral resolution. In CBD, this can be obtained by controlling the shape of the particle beam and the particle velocities.

The production of particle beams is based on the expansion of a particle-gas mixture through a nozzle, generating a sonic or supersonic gas stream [20]. The basic concept of an effusive beam source is very simple: it is an orifice in a very thin wall of a reservoir where the gas or vapour is in thermal equilibrium. The opening is small enough so that the outgoing flow will not affect the equilibrium in the reservoir. If the pressure in the reservoir is low enough, the outgoing flow will be molecular so that the effusion rate and both the angular and velocity distributions of the formed beam can be calculated on the basis of the gas kinetic theory without any assumption [53].

A supersonic expansion can be obtained by imposing a pressure ratio less than $P_b/P_0 = 0.478$ across a convergent nozzle driving an isentropic flow expansion where P_0 and P_b are the stagnation and the background pressures, respectively. The expansion through a convergent nozzle will always take place in a subsonic regime regardless of the amount of the applied pressure ratio. Outside the converging nozzle, depending on the pressure ratio, the flow will supersonically expand to pressures even much lower than the background. A normal shock, known as Mach disc, matches the pressure inside the jet to the background and closes an area called the zone of silence. The location of the Mach disc has been empirically determined as being only a function of the pressure ratio and independent of the fluid nature and nozzle geometry [54].

The sudden free expansion of the flow produces a high outward radial velocity at the beginning of the free jet close to the nozzle outlet. This radial velocity (drag) greatly varies with the radial position both in the jet and at the nozzle outlet. It is weak at the centreline and very strong close to the nozzle wall at the outlet. Hence, in contrast to the particles located in the central regions, those far from the axis are exposed to a strong radial drag. Consequently, the trajectories of particles concentrated on the centreline can remain approximately unchanged, while particles far from the axis may strongly diverge in the free expansion. It should be also noted that the response of the particles to this radial drag is a function of the particle size. The above mentioned

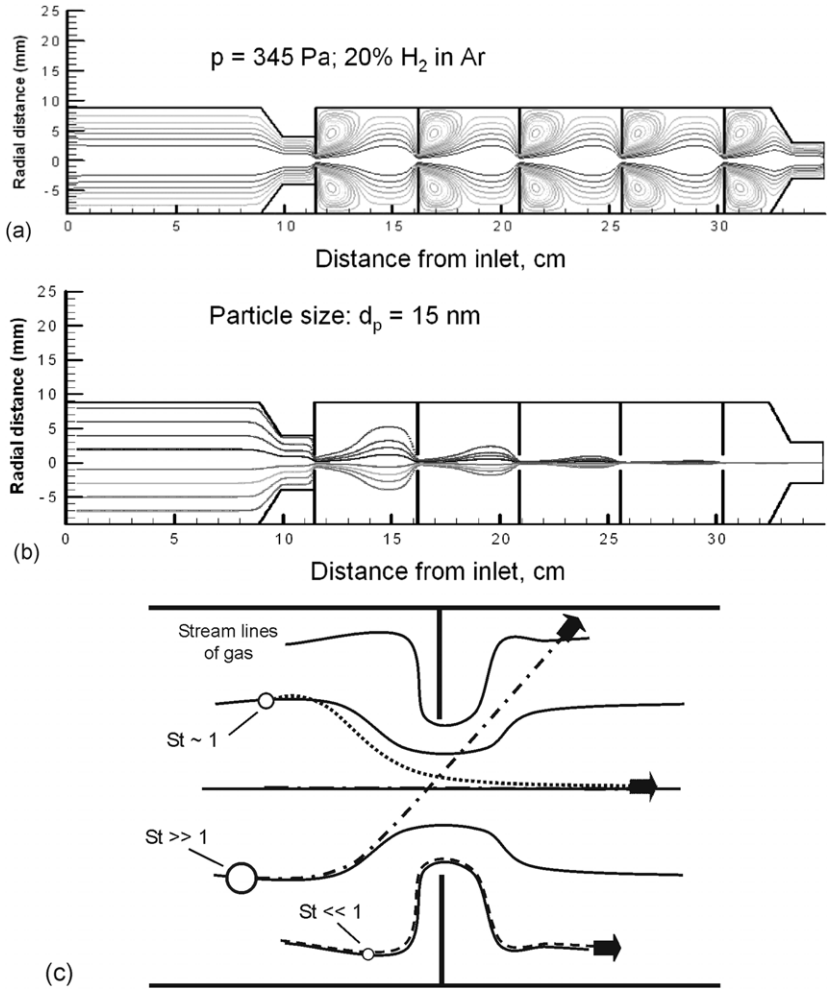

Figure 2. Simulation of the gas flow (*a*) and trajectories of 15 nm particles (*b*) in an aerodynamic lens system according to Gidwani and Di Fonzo *et al* [112, 149]. The particles are concentrated at the centre axis of the lens system, forming a beam. (*c*) Basic principle of aerodynamic size-selection and focusing. The inertia of large particles ($St \gg 1$) exceeds the drag action of the gas, separating the particle trajectories from the gas stream lines and leading to wall deposition. Very small particles ($St \ll 1$) closely follow the flow. Intermediate size particles have trajectories only slightly decoupled from the stream lines, which can be exploited to concentrate them at given positions in the flow-field [29, 66].

radial drag can effectively separate the particles of different sizes especially if they are not concentrated on the centreline. Small particles can follow the expanding carrier gas, while large particles persist on their original trajectories [55, 56].

If the particles can be concentrated on the nozzle centreline, only Brownian diffusion (and lift-force effects in case of non-spherical particles [26, 27]) can perturb/spread the configuration obtained by aerodynamic focusing.

Dirac suggested during World War II that inertial effects in a gas flow can be used for mass separation [57]. One decade later, the experimental evidence of such an effect was obtained by Becker and co-workers [58]. Although the first observations were done in the jet expansion of a supersonic molecular beam source, the subsequent work by Becker was aimed at uranium enrichment in a cascade of aerodynamic separation stages (the 'separation nozzle') the product of which was not a beam of the selected species [59].

In aerosol science, particle separation effects have long been exploited for particulate sampling with impactors. Significant advances in this field have been made pushing the limits of application to nanometre-sized particles and heavy molecules [60]. Regarding an exploitation of these effects for the production of high intensity molecular beams, only very little work was performed in the early times, even though Fenn already recognized in 1963 that the gas mixture in a seeded supersonic beam source is nothing but an aerosol [61]. A probable reason for this neglect is in the complexity and ambiguity of the results of the early experiments, where the background gas was playing a major role [61, 62].

The first attempts to focus particles through supersonic expansions were made by Murphy and Sears [63] and Israel and Friedlander [64]. Dahneke and Flachsbart [65] increased the particle concentration in the core of an aerosol free jet using an extra stream, sheath air, that confines the boundaries of the core jet downstream of the nozzle. In the recent literature, the major development in particle focusing dates back to the work of Liu *et al* [26, 27]. They were the first to produce an enriched stream of particles using only aerodynamic effects induced by nozzles. This was achieved with a system of so-called aerodynamic lenses consisting of successive axisymmetric contractions–enlargements of the aerosol flow passage (figures 2 (*a*) and (*b*)).

The work of Liu *et al* [26, 27] was inspired by the pioneering research carried out by Fernandez de la Mora [66,67] and co-workers who revealed the possibility of particle focusing and the existence of a common focal point for the near-axis particles when expanding an aerosol through a thin-plate orifice (figure 2(*c*)). Unfortunately, particle beams may diverge after a sharp focal point downstream of the nozzle because the gas streamlines diverge due to the sudden gas expansion. The over-exposed images reported by Fuerstenau *et al* [68] visualized the above divergence in aerosol jets expanded through thin-plate orifices. The novelty of the work of Liu *et al* [26, 27] is that they employed thin plate orifices in a confined passage to manipulate the spatial distribution of particles prior to the nozzle and the subsequent expansion in the free jet.

In 1999, Mallina *et al* [69] demonstrated that the beams produced by expansion through capillaries have lower angular spread than those formed by expansion through conical nozzles. This is due to the focalization of particle beams at a point downstream of the conical nozzle and beam divergence afterwards, similar to thin-plate orifices. In capillaries, however, particles asymptotically converge to the focal point, which appears to be inside the capillary, and do not significantly diverge afterwards as the capillary walls confine the gas streamlines.

Goo [70] simulated the aerosol concentration at atmospheric pressure in a cascade of aerodynamic slit lenses followed by a virtual impactor. Soon afterwards, Lee *et al* [71] reported on experiments and numerical simulation of particle focusing at atmospheric pressure. Zhang *et al* [72] repeated the simulations of Liu *et al* [26] with less restrictive assumptions, allowing them to study a wider range of particle sizes. Specifically, they considered the compressibility of the continuous phase as well as particle loss due to wall impact. Zhang *et al* [72] observed that the maximum particle displacement, as well as particle loss, occurs at a particle Stokes number near unity.

Piseri *et al* [56] developed a new type of aerodynamic lens system. By placing an obstacle (a flat plate hereafter called a focuser) upstream of a capillary nozzle, they forced the flow to undergo two 90° turns to reach the nozzle inlet. The spacing between the focuser and the nozzle inlet is the controlling parameter for selecting particles of the desired size (figure 3). In comparison to the aerodynamic lens system of Liu *et al* [26, 27], particles approach the orifice with a more uniform velocity and direction and experience a more uniform and higher acceleration. Furthermore, this new design is less sensitive to the upstream position of the particles (for instance in the cluster source or synthesis chamber). Thus, a broader size range of particles originating from distances farther from the centreline can be focused. The device is very compact, has few components that are easy to machine, and is not subject to critical alignment requirements. The main drawback of this design is the high rate of particle deposition to the wall.

Vahedi Tafreshi *et al* [73] have simulated the performance of the above aerodynamic nozzle in its full three-dimensional geometry. They also considered an axisymmetric model and studied the effects of different operating conditions, spacing and the initial position of particles [74]. They reported that the Brownian diffusion cannot drastically affect the aerodynamic

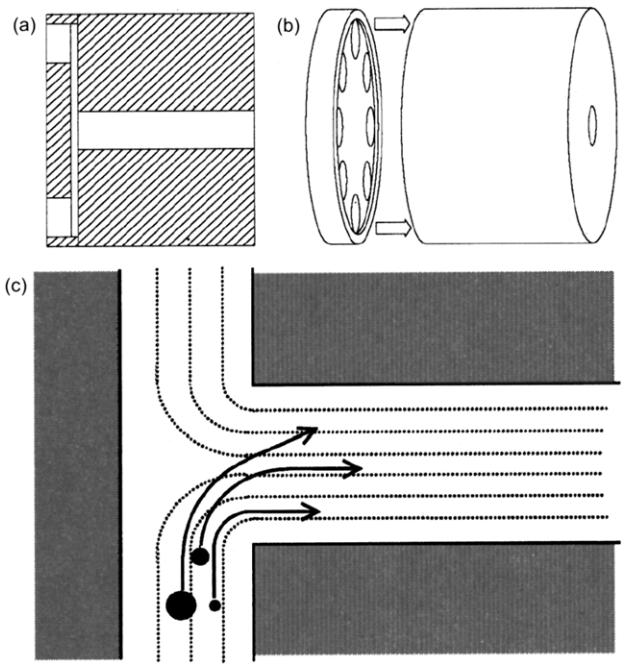

Figure 3. Cross sectional view of the focusing nozzle assembly (*a*), to scale. The narrow gap between the two pieces, where the gas flow is directed towards the nozzle axis can be seen on the left of the figure; (*b*) is a perspective view of the same two pieces (exploded). The focusing mechanism is shown in (*c*); at a given pressure only particles with proper size have trajectories leading to particle concentration close to the nozzle axis. Reprinted from Piseri P, Podestà A, Barborini E, Milani P 2001 *Rev. Sci. Instrum.* **72** 2261–7 [56]. ©2001 American Institute of Physics.

focusing effect of their lens but can broaden the focused beam to some degree (figure 4) [75]. Middha and Wexler [76] recently proposed an aerodynamic focuser with so-called capped-cone geometry that has revealed a certain improvement over the previous designs [73, 74].

Since the invention of aerodynamic lenses by Liu *et al* [26,27], this system has been used in a variety of applications. One example is single particle mass spectrometry for aerosol sampling. The ability of aerodynamic lenses to concentrate the beam on a very narrow near-axis region is of crucial importance for the performance of these instruments where a pulsed laser for particle ionization/vaporization is triggered by the single particle itself.

Mallina *et al* [77] have reported on the capability of variable pressure inlets at the entrance of the lens system to produce beams of selected size ranges. By changing the nozzle source pressure, their design obviates the need for sizing the components in order to aerodynamically focus a special range of particles. Fernandez de la Mora [78] used aerodynamic lenses in a variable-pressure impactor to improve the resolution of an aerosol size spectrometer. Recently, McMurry and co-workers have proposed an aerodynamic lens system to focus nanoparticles smaller than 30 nm [25].

4. Cluster sources

Gas-phase cluster formation processes are characterized by critical parameters such as the number of collisions between

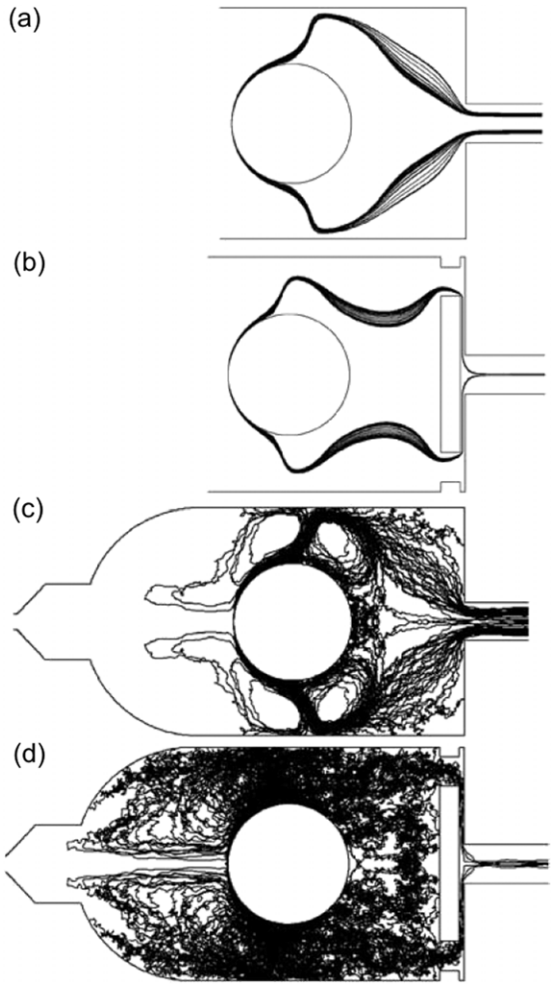

Figure 4. Trajectories of 1.5 nm diameter spherical particles of uniform density inside the PMCS that are released from the cathode surface. The simulations show that without (*a*) and (*b*) and with Brownian motion accounted for, the focuser (*b*) and (*d*) is able to increase the particle number density on the axis. Reprinted from Vahedi Tafreshi H, Piseri P, Barborini E, Benedek G and Milani P 2002 *J. Nanopart. Res.* **4** 511–24, figure 6 [75]. ©2002 with kind permission of Springer Science and Business Media.

aggregating species, collisions between aggregating species and the thermalizing gas and by the method to produce, in a defined volume, the cluster precursors (see section 2.2). Cluster formation takes place in a buffer gas acting as a thermal bath and at the same time as a carrier of the nanoparticles. These two aspects are intimately related so that the pressure inside the particle source determines the condensation efficiency, whereas the pressure gradient affects the cluster extraction and manipulation.

The pressure gradient depends on the pressure of the backing gas, the source and nozzle geometry and the ratio between the pressures inside and outside the source $p_{\mathrm{int}}/p_{\mathrm{ext}}$. The different technical solutions adopted to control these aspects determine the operation principles of different cluster sources and influence their performance in terms of cluster mass distribution, cluster production and extraction efficiency [20].

Cluster sources can be catalogued by considering the regimes governing gas introduction and extraction: continuous or pulsed, effusive or supersonic. At a first glance, continuous production methods coupled to continuous gas flow regimes seem to guarantee an easier and a more efficient production and control of cluster parameters. Actually this can be the case only when very huge gas loads can be handled for ambient pressure aerosol techniques (i.e. flame pyrolysis) [32]. For CBD under vacuum conditions a continuous gas flow must be compatible with stringent vacuum requirements and hence only effusive regimes are of practical interest. Vacuum requirements also affect the pressure attainable in the cluster source that usually should not exceed a few Torr [20]. The critical parameter to control the number of collisions then is the cluster source dimension and geometry.

The realization and operation of pulsed cluster sources appear to be more complicated compared with continuous ones; moreover, they are characterized by a low duty cycle [79]. On the other hand, the reduced gas load has the advantage of allowing the use of a supersonic expansion regime and the compatibility with HV and UHV standards. Moreover, it is possible to control the gas pressure in the source region, where cluster formation takes place, over a very wide range. These aspects are of fundamental importance for applications and in particular for the compatibility of CBD processes with microfabrication and planar technologies [23].

The structure and operation of cluster sources is also determined by the methods used for precursor production. The reader can find many informative reviews describing in detail sources for CBD based on different production methods [80]. Here we will consider cluster sources as possible working tools for the fabrication of nanostructured systems and we will present the aspects related to the interconnection of different parameters (precursor vaporization methods, gas flow, cluster extraction regime, etc) and their importance for the realization of the source hardware for the following methods: (i) joule heating, (ii) sputtering, (iii) laser ablation, (iv) pulsed microplasma cluster source (PMCS) and (v) arc discharge.

4.1. Joule heating

Cluster sources based on joule heating are conceptually simple: in many respects their principle of operation is very similar to that of an atomic beam source [81]. They are based on a reservoir with well-defined exit opening in which a certain vapour pressure of the precursor material must be sustained. The control on the vapour pressure and temperature necessary to induce nucleation is usually realized by mixing the precursors with an inert gas.

Vaporization of the precursors is obtained by joule heating of high-temperature crucibles as in the case of molecular beam epitaxy (MBE) [81, 82]. However, high intensity sources for the production of cluster beams have more stringent requirements. In particular, the vapour pressures are typically about two orders of magnitude higher than those used in MBE which are roughly 10^{-3}-10^{-4} mbar; hence they operate at significantly higher temperatures.

Sources based on joule heating can be used to produce clusters from materials with a low temperature of vaporization. Though, even in this case a complicated construction scheme should be adopted in order to keep the hot oven apart from the

rest of the source. Moreover, the large amount of thermalizing gas necessary to reach condensation conditions makes this kind of source impractical for many applications since the operation is in a continuous regime and results in huge gas loads (figure 5) [83].

4.2. Sputtering

Plasma discharges are of particular relevance for cluster formation. Schematically a discharge consists of a voltage supply that drives current through a low pressure gas between two conducting plates or electrodes [84]. The gas breaks down to form a weakly ionized plasma. Charged particles in the plasma acquire high kinetic energies and collide with the neutrals in the gas, causing the formation of very reactive species. Material sputtering from the plates or electrodes takes place; in this way the electrode material acts as a feedstock of particles injected in the plasma [85].

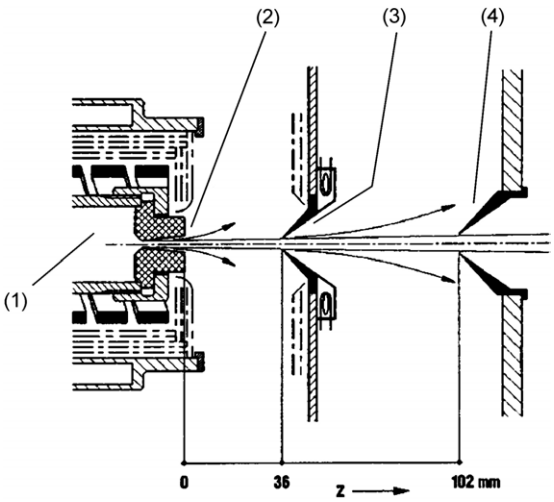

Figure 5. Cluster source based on evaporation by Joule heating. Metal vapour and inert gas expand from the heated high pressure reservoir (1, 2350 K, 500 kPa) out of a conical supersonic nozzle (2). Clusters are formed in the expanding flow. The cluster beam is geometrically confined by a skimmer (3) and a collimator (4). Reprinted from Gatz P and Hagena O F 1995 *Surf. Sci.* **91** 169–74 [83]. ©2005 with permission from Elsevier.

Plasma sputtering offers a method for vaporizing refractory materials without involving the complications of the target heating process. The combination of plasma sputtering with gas condensation was reported in 1986 and then developed by Haberland and co-workers through the use of magnetron sputtering [86, 87]. This source is relatively easy to operate and, in principle, it allows the production of intense cluster beams; however, to date, applications to nano- and microfabrication are scarce.

In figure 6 two different configurations of a plasma-gas condensation cluster beam apparatus are depicted. The general and common features of these systems are: a sputtering chamber, a growth chamber and a deposition chamber. The sputtering of the target material can be obtained with different discharge modes and configurations: dc or rf modes, hollow cathode and magnetron sputtering. The cluster size can be controlled by adjusting the sputter yield, the gas pressure and the volume of the cluster growth region [86,88–90].

The gas pressure inside the sputtering chamber influences the discharge while gas inlet and extraction are critical to determine the nucleation and condensation processes. In order to control the cluster mass distribution, the distance between the sputtering region and the extraction nozzle can be varied. To favour condensation, the source region can be cooled by liquid nitrogen, which however imposes constraints on the source dimensions and geometry [91].

During cluster production, a typical gas pressure in the condensation chamber is 1 mbar, with a gas flow rate of a few hundreds of a standard cm^3 per minute. In order to achieve a high vacuum level of 10^{-7} mbar in the deposition chamber, a high throughput pump is installed in each section of the apparatus. The base pressure of the source is 10^{-8} mbar, while typical pressures during cluster production in the three sections are 10^{-3} mbar, 10^{-4} mbar and 10^{-6} mbar, respectively. This requires a high pressure level, which is found to pose problems to the sputtering operation. Conventional magnetron guns are designed to operate at 10^{-2} mbar, whereas the typical operating pressure in a cluster source is 1 mbar. At such high pressure the plasma is unstable and sputtering on the inside of the magnetron gun can take place [90].

Another important parameter is the geometry of the gas inlet as it affects the pressure in the region where the sputtering

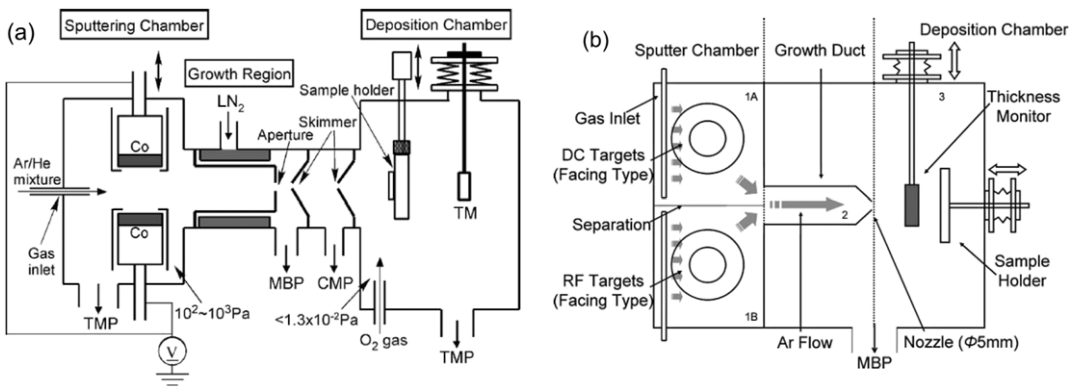

Figure 6. Single (*a*) and double source (*b*) plasma-gas condensation cluster beam apparatus. Reprinted from Sumiyama K, Hihara T, Peng D L and Katoh R 2004 *Sci. Technol. Adv. Mater.* **6** 18–26. [91]. ©2004 with permission from Elsevier.

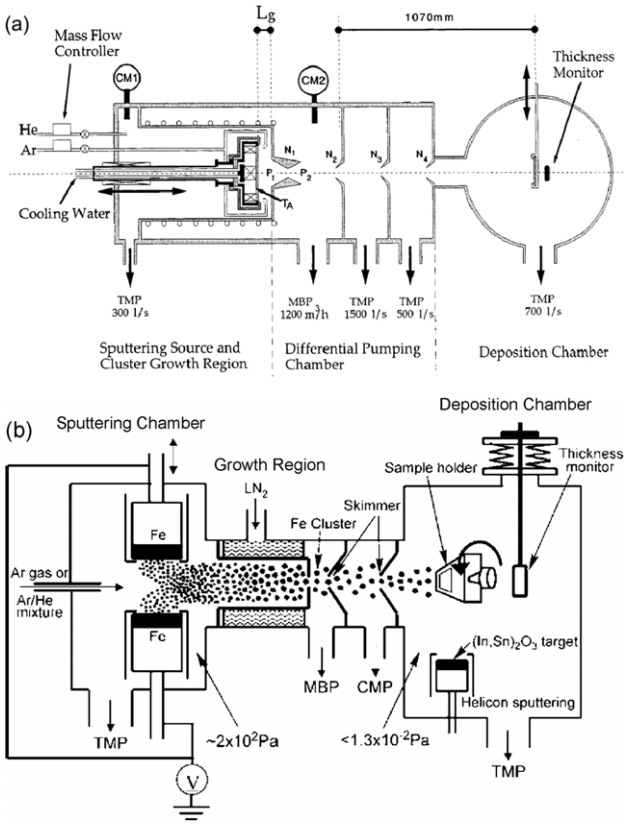

Figure 7. Two configurations of a plasma-gas-condensation type cluster deposition apparatus reproduced from (*a*) Hihara and Sumiyama [88] and (*b*) Peng *et al* [135]. 'CM', 'T_A', 'TMP', 'MBP', and 'CMP' represent capacitance manometers, sputtering targets, turbomolecular pumps, mechanical booster pumps and compound molecular pumps, respectively.

takes place and hence the cluster formation in terms of cluster mass distribution. Sumiyama and co-workers have characterized this aspect in detail [88]. Figure 7 shows two different inlet configurations.

4.3. Laser vaporization

Laser vaporization can generate a high density vapour of virtually any material in a short time interval and in a well-localized volume. By rapid quenching of the plasma, clusters and nanoparticles can be produced [92, 93]. This technique was originally applied to the production of clusters in molecular beams by Smalley and co-workers [94]. Since this pioneering work, laser vaporization has become one of the most common techniques for generating cluster beams especially of refractory materials [20].

The kinetics of aggregation of the plasma produced by laser ablation and the characteristics of the resulting aggregates (density, size distribution, structure, etc) as well as the intensity and stability of the laser vaporization cluster source (LVCS) are influenced by the quantity and type of ablated material, the plasma—buffer gas interaction, the plasma—source wall interaction, and the cluster residence time prior to expansion. High power pulsed solid-state or excimer lasers are used for the vaporization; the pulsed nature of the precursor production makes this approach particularly suited for pulsed gas regimes.

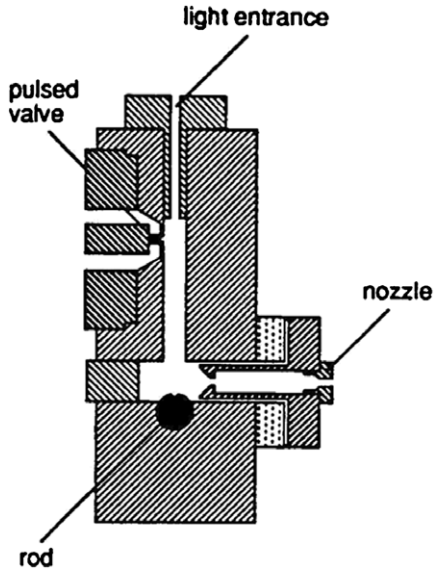

Figure 8. Schematic representation of a LVCS. Clusters are generated by focusing a pulsed laser beam through the light entrance on a target rod of the desired material. An inert carrier gas is pulsed over the rod. Metal clusters are formed and thermalized in the near-sonic flow of the carrier gas as it passes down a thermalization channel before it is expanded through a nozzle. Picture after Milani and deHeer [93].

Since the vaporization volume in a LVCS is very small, the dimensions of the source are significantly smaller compared with hot oven or plasma sources. In figure 8 a schematic representation of a LVCS is shown where the critical parameters affecting the source performance can be recognized.

The light of a high intensity pulsed laser (usually with a pulse length in the order of tens of nanoseconds) is focused onto a target vaporizing a small amount of material into a flow of an inert carrier gas. The inert gas quenches the plasma and cluster condensation is promoted. The mixture is then expanded into vacuum and forms a cluster beam. When a pulsed vaporization takes place it is convenient to operate the LVCS with a pulsed valve for carrier gas introduction. Different geometries have been developed for target mounting and to favour cluster formation and growth prior to the extraction. Originally, Smalley and co-workers proposed a scheme where the inert gas flow was directed through a narrow channel (typically a few mm in diameter). Perpendicular to this channel a hole was drilled to allow the laser to hit a target rod. This geometry does not favour cluster formation, moreover the interaction of the plasma plume with the walls of the source causes instabilities in the operation [94]. Cluster formation can be improved by using long channels or pre-expansion extensions of the nozzle [95]. However, a long channel length allows the metal vapour and clusters to diffuse to the walls and hence be lost.

To overcome these shortcomings, a cavity can be introduced where the vaporization takes place before the channel. This cavity should be properly dimensioned in order to minimize the interaction of the plume with the walls, thereby reducing material deposition, and optimizing heat transfer to the cavity walls by the inert gas. Furthermore, the processes involved in vaporization, cluster formation and thermalization are effectively decoupled from the expansion process [93].

The characteristics of the cluster population are controlled by the local gas pressure during plasma production and the residence time of the particles in the source body. The plasma gas interaction affects not only the final cluster distribution but also the subsequent expansion and beam formation. By monitoring the pressure evolution in a LVCS, it has been shown that vaporization in a low pressure environment produces a large amount of monomers. Increasing the pressure during the ablation results in a shift of the cluster distribution towards larger masses [96].

Different geometries have been used depending on the target shape: when the target is a disc (as for many semiconductor materials), a gear mechanism inducing rotation must be used in order to allow a uniform consumption of the surface of the target. In particular, a hypocycloidal planetary gear assembly has been used to burn out a spirographic path on the target [97]. The disc configuration requires the solution of several problems such as the sealing of the disc-source block interface while keeping the disc moving.

The laser pulse characteristics influence the quantity and the state of the matter removed from the target. Pellarin *et al* [98] have shown that the use of a Ti : sapphire laser (790 nm, 30 ns pulse width) can produce intense transition metal cluster beams over a wide mass range. Deposition rates of 0.2 nm s^{-1} for transition metals have been reported.

LVCS are very flexible and allow the production of metallic, oxide and alloy clusters with a large variety of structures and stoichiometric combinations [80]. The low gas load allows the coupling of LVCS to UHV deposition equipment [80]. On the other hand, the deposition rates are rather low and typically only small areas are covered. This is a serious bottleneck in the use of LVCS for the synthesis of nanostructured materials in view of its applications.

4.4. Pulsed microplasma cluster source (PMCS)

In sputtering-based gas aggregation sources, plasma-assisted vaporization and cluster growth take place in two different regions but in direct succession. Though, stable cluster beams are produced, this class of sources requires huge pumping systems and it is not well suited for supersonic expansions. In pulsed laser vaporization sources (PLVS) the target ablation is confined in a very small volume, thus allowing stability of operation. However beam intensity is the major problem [20].

One of the key factors for improving the performance of cluster sources is the confinement of the ablation plasma in a well-defined region of the target in order to achieve material vaporization with high efficiency and to control cluster growth by the inert gas pressure in that region. Source geometry and dimensions should also be optimized to produce intense and stable cluster beams, while using a relatively low carrier-gas load.

PMCSs represent a combination of different elements typical of sputtering sources and LVCSs [99]. The working principle of PMCSs is based on spatially confined pulsed plasma discharge ablation of a target placed in a condensation chamber. The vaporized species are quenched by a pulse of inert gas and condense to form clusters [100].

Schematically the source consists of a ceramic body with a channel drilled through to perpendicularly intersect a larger cylindrical cavity (figure 9). The channel holds the target to be vaporized which typically is connected to the negative pole of a power source, thus acting as a cathode. The anode can be placed at some location inside the cavity or can also be introduced through the channel, opposing the cathode. A solenoid pulsed valve for introduction of inert carrier gas closes one side of the cavity while a nozzle is located in the opposite cavity wall. The valve, backed with a high gas pressure (typically up to 50 bars), delivers inert gas pulses to the source cavity with an opening time of a few hundreds of microseconds. If the pulsed valve is closed, the source cavity is at the same pressure as the first vacuum chamber. Once the valve opens, the large pressure difference causes the formation of a supersonic gas jet directed against the cathode. A pulsed voltage (typical duration: 50 μs) applied between the electrodes, ionizes the gas and generates a plasma. This is accelerated against the cathode and ablates the material that thermalizes and condenses to form clusters [99, 100]. Due to the formation of a strong pressure gradient close to the cathode surface, an aerodynamic confinement of the plasma is produced in the source cavity and the sputtering process is restricted to a cathode area of less than 1 mm^2, as has been demonstrated by computational fluid dynamics (figure 10) [100].

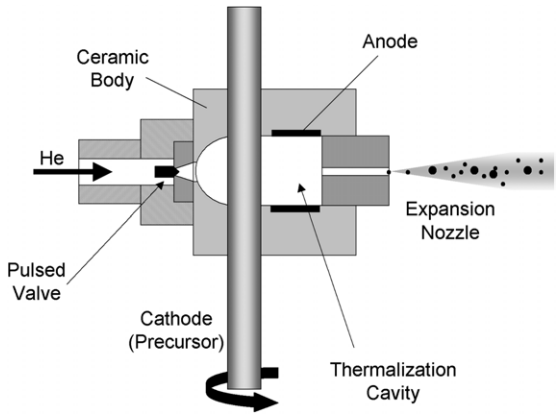

Figure 9. Schematic representation of a PMCS according to Barborini *et al* [99]. Inert gas is introduced through a pulsed valve into a cavity containing the rotating target cathode. When a high voltage is applied between anode and cathode, the material is sputtered from the cathode rod. The precursor vapour condenses into clusters which grow in the thermalization cavity before they are extracted from the source through an expansion nozzle.

These simulations showed how a hypersonic helium jet develops inside the source at the time of the electric discharge, causing the confinement of the ablation plasma, improving the sputtering yield and favouring cluster seed condensation by creating a high pressure region that coincides with the one of ablation. This is crucial to assure a PMCS operation stability and reproducibility that is superior to other cluster sources [56, 101]. Since the volume of the source cavity is very small ($\sim$ 2 cm^3), the source mean pressure rises rapidly after each pulse. The pressure difference across the nozzle drives the aerosol expansion into the adjacent expansion chamber in the form of a supersonic beam.

In general, it is very difficult to obtain experimental information on the temperature and pressure fields inside a PMCS due to its transient flow features, the high temperature and short duration of the discharge and the geometrical

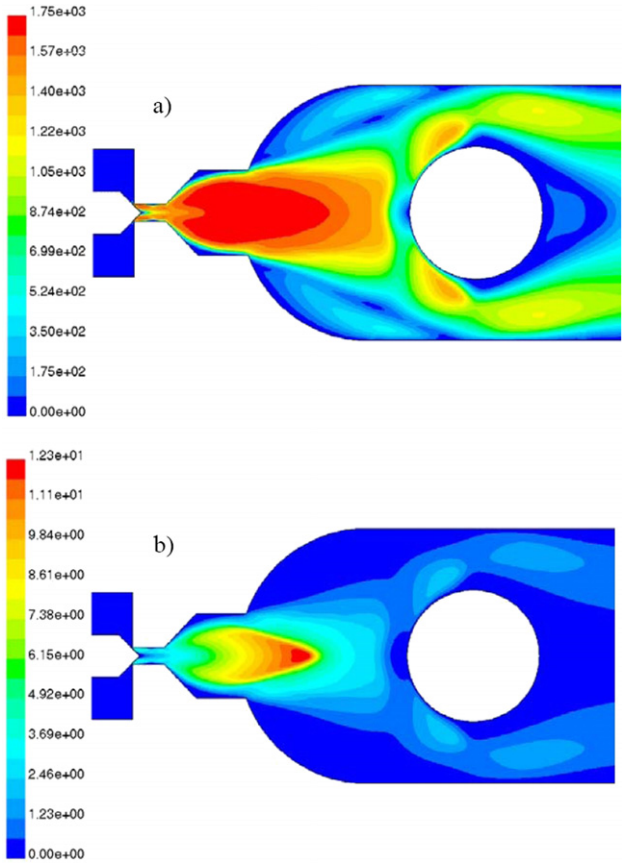

Figure 10. Velocity (*a*) and Mach number (*b*) fields in a PMCS by computational fluid dynamics simulations. It can be seen how a hypersonic helium jet develops inside the source at the time of the electric discharge causing the confinement of the ablation plasma to the region of the jet stagnation point on the cathode rod. Reprinted with permission from Vahedi Tafreshi H, Piseri P, Benedek G and Milani P 2006 *J. Nanosci. Nanotechnol.* **6** 1140–9. ©2006 American Scientific Publishers, http://www.aspbs.com [100].

compactness and complexity of the source cavity. Thus, computational fluid dynamics simulations backed up by experimental data, for instance at the source inlet, and outlet can play a significant role in understanding the fluid and particle growth dynamics inside the source and can assist in improving the design of such systems. Carrying out such computations, Vahedi Tafreshi *et al* [73–75] thoroughly studied the flow inside and exiting a PMCS and revealed the importance of aerodynamic effects in controlling the spatial distribution of particulate phase in the cluster-laden supersonic flow exiting the PMCS.

For a graphite cathode, a lognormal cluster mass distribution in a range from few tens to several thousands of atoms per cluster with an average size at about 1000 atoms per cluster is obtained with the PMCS [56]. By operating the PMCS with a pulse frequency of 5 Hz, deposition rates of 100 h^{-1} over a surface of 1 cm^2 placed at 500 mm from the exit of the nozzle can be achieved. Thus, even thick layers can be deposited by supersonic CBD at room temperature on inorganic and polymeric substrates (figure 11) [56, 101].

PMCSs can be used for the production of refractory material clusters and in particular of transition metal-oxides and nitrides [101, 102]. Using cathodes consisting of various

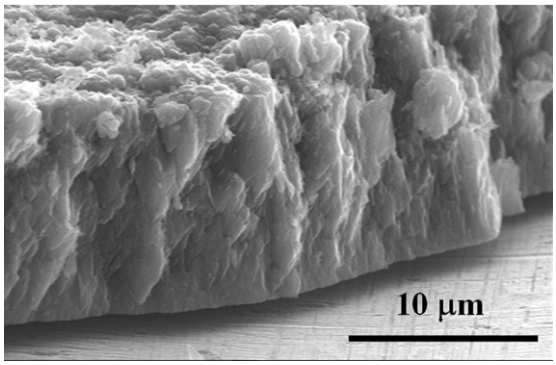

Figure 11. Scanning electron micrograph of a thick film formed by carbon nanoparticle deposition using CBD with PMCS.

chemical species, mixed clusters can be obtained in order to deposit nanocomposite films at high deposition rates over a large area. PMCSs have been used for the production of devices such as supercapacitors [103], sensor arrays [23, 104] or high-throughput screening arrays for biological applications [105]. PMCSs can be equipped with focusing devices as described in section 3 in order to further improve cluster beam intensity and patterning capabilities [24].

4.5. Arc discharge

A pulsed source of highly ionized metal plasma is the electric arc, consisting of a discharge between two conductive electrodes. The arc regime is characterized by a relatively low cathode potential fall in contrast to a glow discharge where the potential drop is several hundred volts [84]. This is due to different mechanisms underlying cathode emissions: arc cathodes emit a large electron current as a result of thermionic, field electron and field emission [84]. Arc discharges are characterized by large currents (1–10^5 A), causing a considerable heating either of the entire cathode or of a small area for short time intervals, thus inducing vaporization of the electrode material. The vaporized material, ejected in various forms and forming a plasma between the electrodes, can undergo condensation into clusters. The presence of a buffer gas surrounding the electrodes influences the plasma expansion from the electrode spots and also changes the behaviour of the arc and the role of the electrodes.

The application of an arc discharge to the production of supersonic cluster beams was originally proposed by Meiwes-Broer and co-workers in 1990 [106, 107]. The pulsed arc cluster ion source (PACIS) was conceived as an alternative to laser vaporization sources: the vaporization of the precursor electrode being obtained by a pulsed high current discharge between two electrodes. The plasma produced in this way is mixed and thermalized by an inert gas jet between the electrodes that is introduced through a pulsed valve. A schematic representation of the PACIS is shown in figure 12. Two cylindrical electrodes of a few millimetres in diameter are placed in an insulator block (usually Macor or boron nitride) with 1–2 mm spacing in between them. A pulsed valve that can be synchronized with the firing of the discharge supplies pure or mixed gases. The gas reaches the electrode gap through a channel of variable diameter and length (in the design of Siekmann *et al* [107] the channel has a diameter of 1 mm and

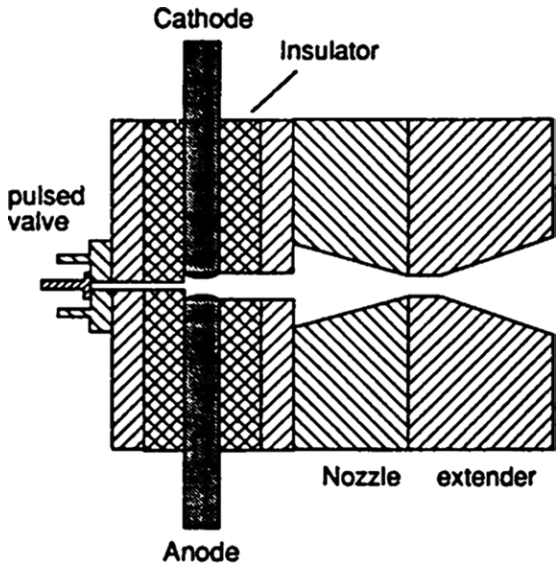

Figure 12. Principle of the PACIS: Two metal rods are mounted opposite to each other in a ceramic block. A pulsed arc discharge produces a plasma which is flushed by a carrier gas pulse through a nozzle into high vacuum. No additional ionizing agent is needed to charge the clusters. Figure after Ganteför *et al* [106].

a length of 10 mm). The plasma produced by the discharge and mixed with the carrier gas travels through a larger channel (2 mm diameter, 10 mm length) and it expands into vacuum or reaches a subsequent 'mixing chamber' characterized by a variable volume and shape [108, 109], which acts as a thermalization zone in a way similar to the one discussed for LVCSs.

Several parameters influence the PACIS performance in terms of produced species, stability, and intensity: nucleation and neutralization processes are controlled by the gas dynamics in the source body and by the nature of the discharge. The geometry of a pulsed arc source can be considered in a way similar to that of LVCSs. In particular, channels and volumes inside the source should be designed to avoid any interference between the plasma and the source walls. For an arc source, a further requirement is the electrical insulation of the electrodes from the rest of the source body. The relevant gas pulse characteristics are duration and intensity: the duration determines the quantity of gas introduced into the source chamber and the pressure inside the source. In principle, by varying the delay between the valve opening and the discharge, it is possible to change the gas dynamics between the electrodes and hence to influence cluster growth.

A continuous version of the arc source has been proposed: it is based on an arc discharge in a hollow cathode [80]. The produced clusters are mainly ions. With this source, clusters of magnetic materials have been studied after size selected deposition in UHV [80].

5. Patterning and coupling to planar technologies

The fabrication of functional devices based on nanostructured materials requires the ability to assemble nanoparticles in micrometre and sub-micrometre patterns with high precision and compatibility with planar technology. Physical and chemical deposition techniques are used for the patterning of semiconductor, metallic and polymeric films and for the production of dot arrays. These techniques require putting resists or stamps in contact with a substrate that undergoes different pre-or post-deposition etching or thermal treatments.

The effect of such treatments on cluster-assembled materials has not been investigated systematically; however, several problems due to the porosity and 'granularity' of nanostructured materials can be expected. For nanostructured films, a non-contact patterning would thus be highly desirable, and, in principle, it would be viable e.g. by depositing particle beams on a substrate through a stencil mask. To be useful for practical applications this process must fulfil several requirements such as high lateral resolution, large area deposition, high deposition rate, surface finish and compatibility as well as low temperature processing.

Supersonic cluster beams are characterized by high directionality, collimation and intensity and thus are well suited for patterned deposition of films through stencil masks that are placed into the beam in front of the substrate (figure 13) [23, 110]. A remarkably high step sharpness could be obtained as reported by Barborini *et al* [110]: a width of 450 nm using a mask placed at 0.33 mm from the substrate. The profile of the mask is reproduced even in its sub-micrometre features. By the use of micromachined masks patterns with micrometric pitch can be reproduced in the deposited material. Patterning over larger areas can be realized by source rastering at the cost of a little reduction in the attainable resolution. Rastering produces as a matter of fact an effective broadening of the source extension thus leading to larger penumbra regions; as the typical spot size of a focused beam is about 6 mm at 300 mm distance from the source, the maximum virtual extension of the source is limited to this size. Moreover, the use of alignment stages controlled by piezoelectric actuators should also allow the fabrication of structures with high definition and controlled shapes.

Structures with high aspect ratio and controlled shape, arranged in ordered arrays can be created on any kind of substrate. For instance, Milani and co-workers deposited patterns on silicon, aluminium, copper, stainless steel and polyethylene [111]. Structures with heights up to several tens of micrometres could be grown on metallic and polymeric substrates while heights of several micrometres were realized on silicon. The lateral resolution was in the sub-micrometre range [56]. Thus, micrometre-size objects with a structure and porosity on the nanoscale could be created, as the low deposition energy in CBD from supersonic beams typically does not lead to compaction or fracture of particles upon impact on the substrate.

The lateral resolution does not depend so much on the sharpness of the mask edges as on the beam collimation. Supersonic expansions have a higher collimation compared with effusive beams; however, clusters in supersonic beams can still have a non-negligible thermal divergence and a broad mass distribution [56]. In order to study the effect of the transverse cluster velocities on the step sharpness, films were deposited at different supersonic conditions by masking part of the substrate with a straight edge mask. Assuming the film thickness as a measure for the beam flux, integrated over the deposition time, the profile of the step obtained with the mask

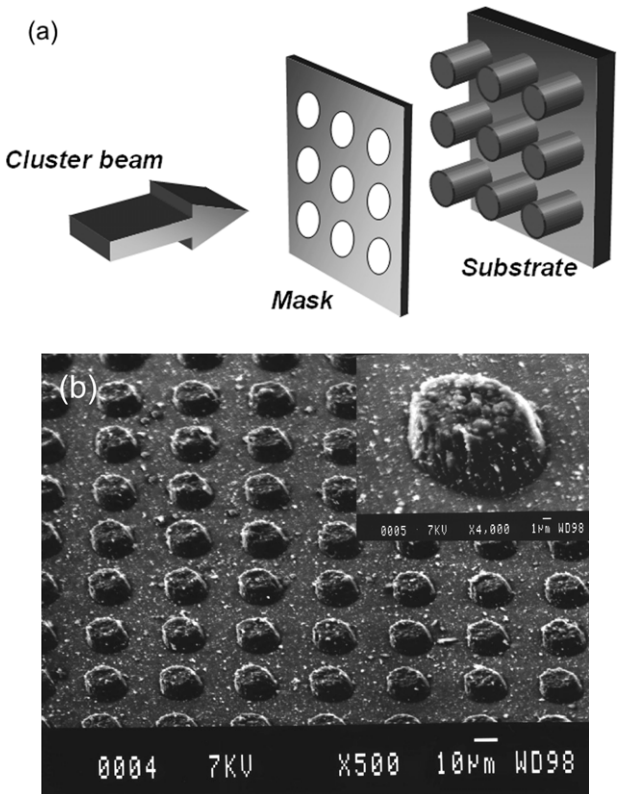

Figure 13. Schematic showing the deposition of patterned films (*a*) by placing a hard mask into the particle beam at some distance from the substrate. The scanning electron micrograph (*b*) shows a carbon film obtained by this method with CBD. Adopted from Barborini *et al* [110].

is affected by the distribution of cluster transverse velocities. With a standard supersonic beam the step is very noisy and not well defined. In order to increase the step sharpness one should increase the Mach number of the beam but this will require a huge pumping system [56]. The use of a focusing nozzle can circumvent this problem by concentrating the clusters on the centre beam, keeping intact the other expansion parameters. Di Fonzo *et al* [112], for instance, used an aerodynamic lens assembly for the deposition of patterned microstructure films.

Mazza *et al* [23] fabricated micropatterned sensing arrays by supersonic CBD. By one-step CBD a total of 210 sensors was manufactured on an alumina wafer where a 14 × 15 array of interdigitated gold electrodes had been previously microfabricated (figure 14). A custom-made stencil mask was superimposed to the substrate in order to deposit the film only in the area of the interdigitated electrodes.

The biocompatibility of cluster-assembled titania films [105] suggests patterned deposition by CBD and stencil masks in the fabrication of microarrays for proteomics, genomics and post-genomic applications.

If arrays of individual clusters rather than nanostructured films are to be produced, these nanoparticles have to be pinned to the surface to prevent particle diffusion and subsequent aggregation. This can be achieved if the impact energy of the cluster is high enough to displace at least one surface atom of the substrate, thus creating a reactive site that binds to and immobilizes the cluster [113–115].

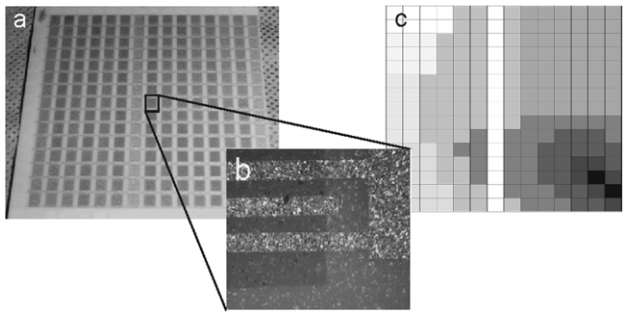

Figure 14. (*a*) Array of 210 titania gas sensors made by CBD onto an alumina wafer with interdigitated gold electrodes (*b*) employing hard mask patterning [23]. The layer thickness represented by the grayscale in figure 14(*c*) varies between the sensing elements leading to individual different gas sensing performance.

Other patterning mechanisms have been developed for deposition of gas phase nanoparticles; we review them briefly here for a comparison of the resulting systems, which show strong similarities with those obtainable by CBD, although the deposition regime is completely different. These mechanisms rely on low-range attractive forces, i.e. thermophoretic and electrostatic forces effective in the moderate velocity regime and mostly in the presence of diffusion. Electrostatic forces are used in designing electrostatic precipitators which capture charged particles in the gas flow through a collector chamber. In a simple electrostatic precipitator, a high voltage difference is applied to two plates; the plate connected to the positive pole of the power supply charges the particles while the negative grid attracts them. An electrostatic precipitator was used for example by Camata *et al* [116] for the deposition of nanoparticles smaller than 6 nm. Jacobs and Whitesides [117] have produced submicron patterns of trapped charges on thin-films of electret polymers (polymers which have the ability to retain electrical charge or polarization) using flexible electrically conductive electrodes. They could pattern areas as large as one square centimetre with trapped charges at a resolution better than 150 nm in less than 20 s which showed a promising application for high-resolution charge-based printing. Creating charge patterns using (polydimethylsiloxane) PDMS stamps, Krinke *et al* [18, 19] developed a parallel process for deposition of monodisperse singly charged nanoparticles on oxidized silicon surfaces. With their technique, they deposited gas-phase nanoparticles on a substrate to form nanowires with diameters as narrow as 100 nm and spaced 2000 nm apart. A numerical simulation of the deposition of charged nanoparticles in the size range below 100 nm in a homogeneous electric field on flat substrate surfaces was presented by Krinke *et al* [118]. They calculated the nanoparticle trajectories by solving the Langevin equation of motion taking into account the influence of the electric field, the particle charge and van der Waals interactions as well as Brownian diffusion. Trajectory calculations were compared with experimental results obtained from scanning electron microscopy analysis of deposition patterns. Krinke *et al* [118] concluded that in the case of uncharged particles on the substrate, any deposited particle attracts incoming particles, which leads to an enhanced agglomeration on the substrate rather than a random distribution. In the case of charged

particles on the substrate, the agglomeration on the substrate can be reduced.

Thermophoretic forces act on particles in the gas phase when a temperature gradient is present that results in a momentum imbalance between the warmer and colder side of the particle. Such forces can be used for nanoparticle deposition and patterning. Ostraat *et al* [17], for example, designed a two-stage aerosol reactor with deposition chamber in order to integrate Si/SiO_2 nanoparticles into memory devices. Nanoparticle deposition was based on thermophoretic forces. Their deposition chamber was designed to produce a controllable particle density profile along the substrate where particles were deposited uniformly. Ostraat *et al* [17] also simulated the flow of aerosol nanoparticles subjected to thermophoretic forces in their deposition chamber using a commercial software.

6. Applications

Clusters and nanoparticles of metals oxides, carbon and semiconductors have been extensively studied in the gas phase with particular attention to their electronic properties. Using CBD, nanoparticles have been deposited on various substrates to study the influence of flux, kinetic energy, mass distribution and other parameters on the particle–surface interaction and on the post-deposition particle organization. Apart from electronic properties, applications of cluster-assembled films as well as individual clusters in optics, magnetism, gas sensors, catalysis and biotechnology are briefly presented in this section.

6.1. Microelectronics, optoelectronics and optics

Semiconductor-based nanocrystalline materials are the subject of considerable interest driven by their optical and electronic properties [6]. Group IV-based structures, for example consisting of Ge and Si nanocrystals embedded in matrices or free-standing, exhibit visible photoluminescence that is sensitively dependent on the particle size and size distributions [119]. Since CBD allows a good control over particle sizes and shapes it may offer some advantages in the preparation of nanocrystalline samples over more conventional techniques for the preparation of porous silicon which are based on electrochemical etching or plasma enhanced chemical vapour deposition from an rf discharge of silane [119].

An intense source of silicon particles that were studied for their photoluminescence has been realized by Ehbrecht and co-workers [120]. Silicon cluster molecular beams were produced by using a gas-flow reactor where SiH_4 is decomposed by continuous or pulsed CO laser irradiation followed by expansion into a molecular beam apparatus. Thin nanostructured films of size-selected Si nanocrystals could be grown, for example, on sapphire substrates by combining the CBD technique with a velocity selector, namely a fast spinning chopper [121]. Deposition through hard masks has also been exploited to shape the beam and manufacture structured thin films of silicon quantum dots (figure 15) [122].

Strong visible photoluminescence of the Si nanocrystals upon ultraviolet radiation was found to be dependent on cluster size and could be explained on the basis of quantum

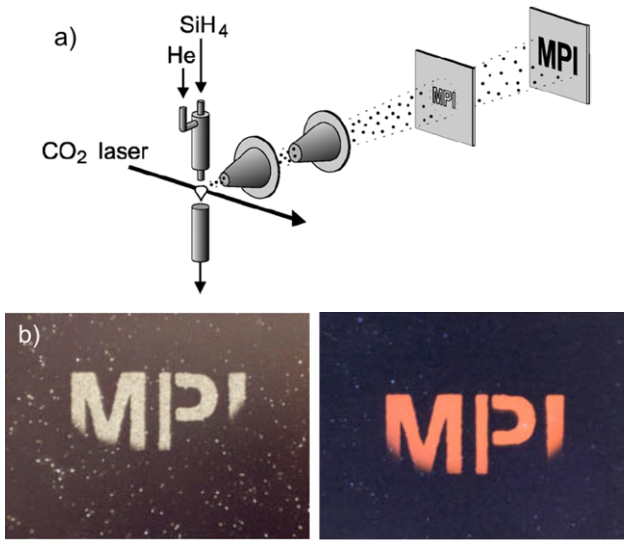

Figure 15. (*a*) Schematic view of the gas-flow reactor where SiH_4 is decomposed by continuous or pulsed CO laser irradiation followed by expansion into a molecular beam apparatus. The beam of photoluminescent silicon quantum dots was deposited though a mask with the letters 'MPI'. Figure 15 (*b*) shows the 3 mm high letters under normal (top) and UV-light (bottom) illumination. Figures reproduced from Huisken *et al* [122].

confinement [123]. Voigt *et al* [124] investigated the growth of ∼78% porous thin films of size-selected Si nanocrystals in detail and compared it with Monte Carlo computer simulations. Simultaneously with film growth they recorded charge transport in a coplanar contact arrangement that showed three regimes: (i) negligible contribution at the beginning of film growth due to missing connections, (ii) a percolation type of superlinear increase of current with exponent 3/2 and (iii) linear increase with further film thickness. Furthermore, Voigt *et al* [124] found that clusters of agglomerated Si nanocrystals in the film conserve the electronic properties of the single nanocrystals.

The production of silicon nanoparticle-based floating gate metal oxide field effect transistors was the focus of Ostraat *et al* [17] who managed to design a gas phase nanoparticle synthesis reactor system that is compatible with silicon manufacturing technology (figure 16). Silicon nanoparticles were first synthesized by thermal decomposition of silane and then passivated by surface oxidation in an ultraclean (transition metal contamination $<10^{10}$ atoms cm^{-2}) two-stage aerosol process reactor. Product particles were directly deposited on a 200 mm silicon wafer.

Ostraat *et al* [17] managed to overcome any concerns regarding particle contamination in microelectronic device fabrication, as particles typically create defects leading to device failure and introduce transition metal contamination that degrades performance. They successfully demonstrated that gas phase nanoparticle and cluster production can be integrated with silicon-technology based microelectronic device fabrication.

Nanostructured carbon systems have been proposed as promising materials for electron field emission applications such as for the production of stable and inexpensive cold flat cathodes, as they might be superior to conventional

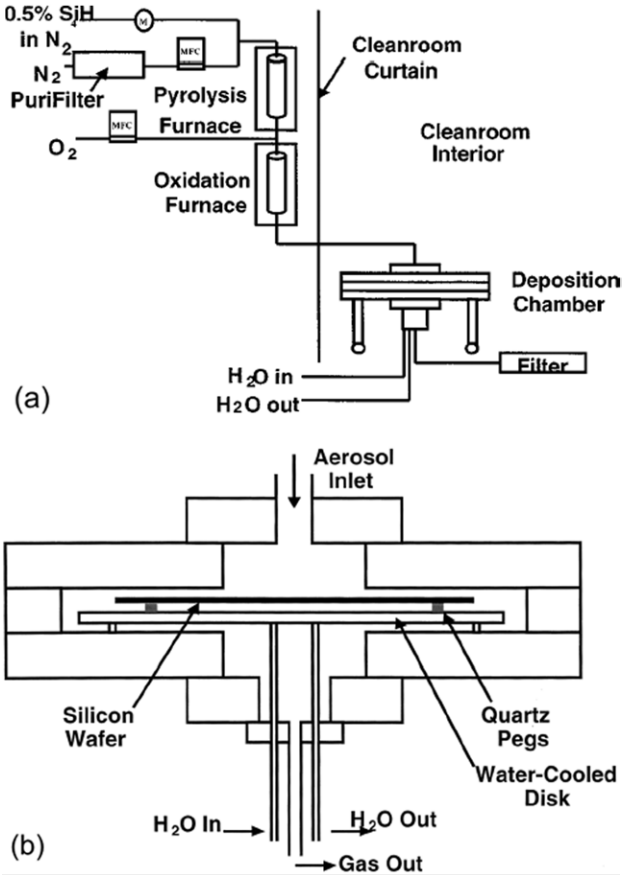

Figure 16. (*a*) Experimental set-up showing the ultraclean aerosol reactor and deposition chamber used by Ostraat *et al* [17]. The deposition chamber (*b*) is housed within a class 100 clean room and allows controlled thermophoretic deposition of nanoparticles onto a 200 mm silicon wafer. Pictures reproduced with permission from Ostraat *et al* 2001 *J. Electrochem. Soc.* **148** 265–70 [17]. ©2001 The Electrochemical Society.

materials in terms of extraction fields, current densities and site emission densities [125]. Using supersonic CBD, Ducati *et al* [125] produced such carbon films on double polished *n*-doped single crystal silicon substrates. They observed that samples heated during deposition showed a stable and reproducible emission, a threshold field as low as $4\,\mathrm{V\,mm^{-1}}$ and a saturation current density of the order of $0.5\,\mathrm{mA\,cm^{-2}}$. It was found that the presence of graphitic particles in the films substantially enhances the field emission performance. Working on patterned films (arrays of micrometric dots made by deposition through hard masks) in the ball-tip anode configuration, a localized effective conditioning could be obtained which led to an emission site density of $5 \times 10^4\,\mathrm{cm^{-2}}$.

Nanostructured carbon films made by supersonic CBD over large areas were applied also for energy storage in supercapacitors (figure 17) [103, 126]. The carbon film electrodes showed a high power density of $500\,\mathrm{kW\,kg^{-1}}$ and can be deposited at room temperature on thin foils, thus ensuring compatibility with actual manufacturing processes for supercapacitors.

Masenelli *et al* [127] investigated luminescence and other fundamental properties of films resulting from the deposition of Eu^{3+} doped Gd_2O_3 clusters by low energy CBD. The

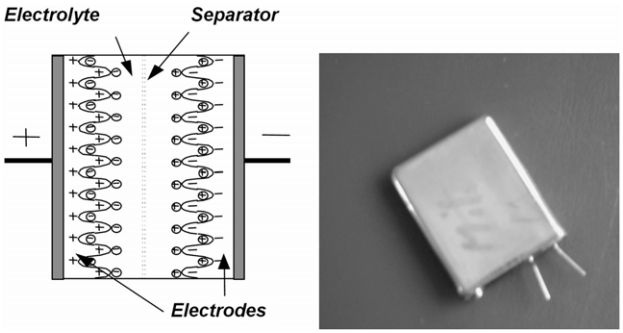

Figure 17. Schematic view of a double-layer supercapacitor (left) and picture of a prototype based on nanostructured carbon deposited by CBD (right). Dimensions: $30 \times 20 \times 4\,\mathrm{mm^3}$, weight: 6.3 g, capacitance: 200 mF, equivalent series resistance: 24 Ω. Reprinted from Bongiorno G *et al* 2006 *J. Mater. Sci. Mater. Electron.* **17** 427–41, figure 17 [126]. ©2006 with kind permission of Springer Science and Business Media.

luminescence spectrum of pure particles with BCC structure for diameters as low as 2.8 nm was reported to be very different from that of bulk material and showed a broad peak at around 625 nm. As with larger nanoparticles, gap widening with the decrease of particle size was observed for clusters with a mean size of 3.2 nm and 2.8 nm. Crystal field symmetry breaking induced by the surface was suggested to be a major mechanism controlling the light emission spectrum. Contamination from air was found to modify the luminescence of the Eu^{3+} ions due to hydroxide formation, suggesting the requirement of a passivating coating of the clusters.

Kreibig and Vollmer [128] give a comprehensive report on the optical properties of metallic clusters deposited on surfaces or embedded in matrices. Noble metal clusters and noble metal cluster alloys embedded in transparent matrices have been prepared by CBD to study the dependence of their optical properties on cluster size and stoichiometry. UV-vis optical properties were investigated for copper, gold and silver clusters (diameter range 1–5 nm) produced by a laser vaporization sources and deposited in an alumina matrix. Also, embedded mixed transition metal/noble metal clusters were characterized [129–131].

Whangbo and co-workers [132] deposited 120 nm thin ZnO films on Si (100) by reactive ionized CBD. Using an evaporation source, Zn clusters were deposited at room temperature on the substrate and oxidized by purging oxygen over the film surface. Electrical and optical film properties were analysed in view of possible applications as surface acoustic wave bandpass filters, optical waveguides, laser deflectors, transparent conducting oxide coatings, gas sensors and varistors. The resistivity of the films was below $10^{-2}\,\Omega\,\mathrm{cm}$, the optical transmittance was about 90% in the visible region, and the band-gap energy was 3.23 eV. Similarly, Zhao *et al* [133] fabricated nanocluster-assembled ZnO thin films by nanocluster-beam-deposition and characterized their optical properties. ZnO nanoparticles were produced with a magnetron sputtering gas aggregation source. The average particle size was around 6 nm with the corresponding absorption edge located at 3.84 eV and UV emission at 3.32 eV, respectively. After the films were annealed in air for 2 h, the shoulder in the absorbance spectra became steeper

and the intensity of UV emission in the photoluminescence spectra became stronger due to the enhanced crystallinity. Redshifts were observed in the evolution of absorption edge and UV emission with increasing annealing temperature—being ascribed to the quantum-size effect.

The formation of iron silicide thin films by CBD to be used as thermoelectric materials was investigated by Kizaki *et al* [134]. Therefore, Fe and Si precursors were vaporized into inert gas using a DC electric arc heat source. The aerosol formed in the colder regions of the source chamber was expanded through a nozzle into the deposition chamber into which a controlled stream of oxygen could be introduced. Alternatively, two separate sources (Fe and SiO) were employed, the beams of which were focused on the substrate. After post-deposition annealing in Ar, the films produced by the latter method exhibited a Seebeck coefficient and electric conductivity very close or superior to those of the corresponding bulk material.

Aiming at the development of new multifunctional devices, Peng *et al* [135] managed to produce nanostructured films that simultaneously exhibit high optical transmittance, low resistivity and room temperature ferromagnetism. This was achieved by combining beam deposition of magnetic Fe clusters with sputtering of indium–tin oxide (ITO) in one apparatus. Thereby, a $\sim$ 10 nm Fe cluster layer was embedded into the ITO matrix. The material had about 90% optical transmittance, a resistivity in the order of $10^{-4}\,\Omega\,\mathrm{cm}$ and showed ferromagnetism at room temperature.

6.2. Magnetic applications

The large body of work carried out in this field was recently reviewed in this journal by Binns and coworkers [136] and by Sumiyama and coworkers [91]. Thus, we refrain here from a new review of this topic and will only point out the recent work of Qui *et al* [137] as it shows how CBD could enter mass production of thin films. Using CBD, they developed a process for fabrication of ultra-high density recording tape media. In this field, new cost-effective fabrication techniques are needed to increase the cost advantage of magnetic tapes over disc-type storage media. In the approach of Qui *et al* [137], magnetic CoPt nanoparticles with a mean diameter of 5.2 nm were generated through gas-phase aggregation in a magnetron sputtering source. Nanoparticles were then expanded into a conditioning chamber equipped with an infrared heater for recrystallization before they were deposited at room temperature on polymer substrates. Using co-sputtering, a thin carbon overcoat was deposited following the nanoparticle deposition, which stabilized the nanoparticles both mechanically and chemically. The so-formed nanocomposite films were then applicable as tape media (figure 18).

6.3. Gas sensors

Apart from wet chemistry methods, sputtering, laser ablation and gas phase condensation routes have been widely applied in the production of solid-state gas sensing devices, as is apparent from the tabulation of Kennedy *et al* [138] for tin oxide sensors. Today, the focus is on combined processes for synthesis and direct deposition, ideally without thermal after-treatment, but

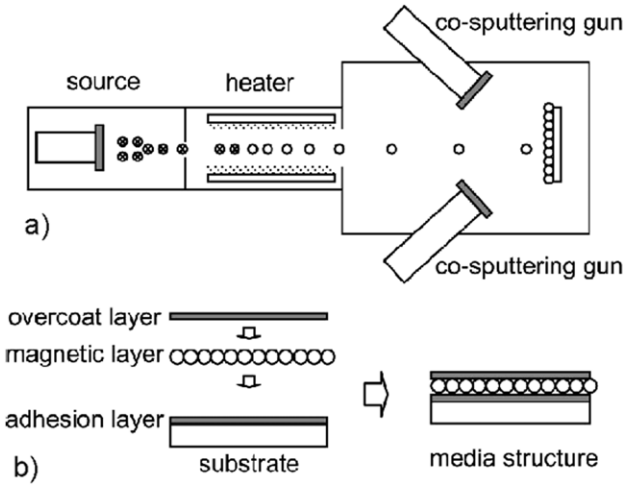

Figure 18. (*a*) Schematic illustration of the integrated system for deposition of magnetic nanoclusters with magnetron sputtering source, infrared heater for recrystallization and co-sputtering guns for deposition of a thin carbon overcoat on the deposited magnetic layer (*b*). Pictures reproduced from Qui *et al* [137].

with integrated in-flight nanoparticle manipulation such as size selection, annealing, focusing and positioning. Thus, existing technologies have been advanced and new processing routes have entered the field, such as combined flame synthesis and direct thermophoretic deposition of highly crystalline Pt-doped tin oxide nanoparticles on sensor substrates [139]. The process resulted in 10–40 μm thick films of high (98%) porosity and 10 nm grain size which were applied in CO sensing.

Kennedy *et al* [138,140] coupled a gas phase evaporation–condensation process for tin oxide nanoparticles with an in-flight annealing zone and a differential mobility analyser to deposit size selected nanoparticles of 10–35 nm on interdigitated sensor substrates by electrostatic precipitation. CBD was employed to fabricate 1–10 μm nanostructured carbon films for humidity sensing (figure 19) [104,126]. The capacitive-type sensors were tested at relative humidity of 10–70% and favourably compared with commercial devices. Mazza *et al* [23] produced libraries of gas sensors for volatile organic carbon based on titania films deposited by CBD on microfabricated substrates using stencil masks. A total of 210 sensors were made in one-step on an alumina wafer with a 14x15 array of interdigitated gold electrodes. Gradients in the anatase/rutile phase composition across the sensor array resulted in individual sensing elements with different performances. By using a combinatorial approach, such an array can give more reliable information than a single sensor.

6.4. Catalysis

Monosize clusters deposited on inert surfaces constitute an ideal model system for studying heterogeneously catalyzed chemical reactions and for gaining fundamental insight in the dependence of product selectivity on the catalyst size. CBD has been used frequently to obtain such model catalysts. A typical experimental set-up has been reported by Heiz *et al* [97] who generated clusters by high frequency laser vaporization and subsequent supersonic expansion of the metal vapour. Cluster generation was followed by mass selection

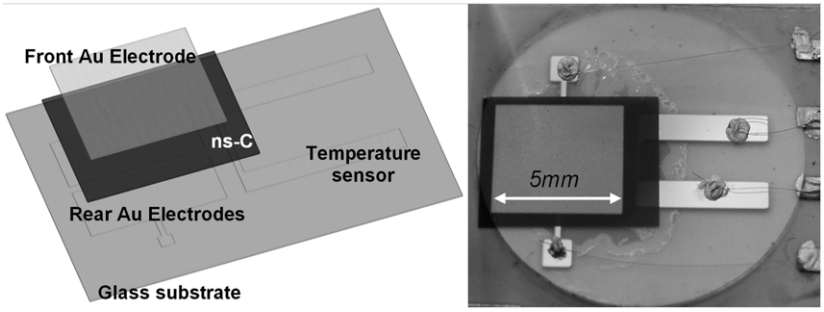

Figure 19. Sketch of the layers composing a capacitive humidity sensor (left) and picture of a capacitive sensor based on nanostructured carbon (right). Two serial capacitors are realized by first evaporating two rectangular Au electrodes (rear electrodes) on a glass substrate; the deposition of the ns-C film has then been carried out onto the rear Au electrodes to produce the dielectric layer, and a thin and permeable Au layer electrode was evaporated on top. A gold thermoresistance sensor is buried under the ns-C film in order to measure the temperature of the device. Reprinted from Bongiorno *et al* 2006 *J. Mater. Sci. Mater. Electron.* **17** 427–41, figure 19 [126]. ©2006 with kind permission of Springer Science and Business Media.

using a quadrupole mass spectrometer and UHV deposition on thin oxide films grown on metal single crystals. The equipment of Heiz *et al* [97] was equipped with in situ FTIR, temperature desorption and Auger electron spectroscopy and was used to study CO on Ni clusters on thin MgO films. Abbet *et al* [141] used a similar source for generating size selected clusters of Ni, Si and Au to be used as monodisperse model catalysts. Specifically, they investigated the adsorption of CO on Pd atoms and CO oxidation on Au clusters. Aizawa *et al* [142] used this type of equipment to investigate deposition dynamics and chemical properties of size-selected Ir clusters on TiO_2, focusing on CO adsorption and desorption. Noble metal clusters of Pd [143] and bimetallic Pd–Pt [144] were deposited on graphite and alumina substrates, respectively, employing laser vaporization and CBD. Both cluster types were employed as model catalysts for studying the hydrogenation of unsaturated hydrocarbons.

Anpo and co-workers intensively studied cluster beam methods to produce various photocatalysts: Ti–Si binary oxide thin film photocatalysts for decomposition of NO into N_2 and O_2 under UV light irradiation [145], Pt/TiO_2 for photocatalytic oxidation of acetaldehyde with O_2 under UV light irradiation [146] and combined CBD–metal ion implantation for doped TiO_2 photocatalysts [147]. A layer of V-ion-implanted TiO_2 on quartz substrates showed photocatalytic decomposition of formic acid even under visible light radiation [147].

6.5. Biotechnological applications

Palmer and co-workers [114, 148] immobilized proteins (GroEL chaperonin molecule from *Escherichia Coli,* pHAT-GFP and Human Oncostatin M protein molecules) on individual Au clusters that were pinned to a graphite substrate. The clusters were created with a magnetron sputtering, gas aggregation cluster beam source and size-selected with a time-of-flight mass spectrometer. Immersion of the Au-cluster decorated substrate in a buffer solution containing protein molecules resulted in preferential binding of the proteins to the Au clusters, as was witnessed by AFM imaging. Thus, well-separated arrays of immobilized proteins could be produced. This technique would permit single molecule optical studies in which only one protein was present in the field of view of a microscope, representing the ultimate limit in biochip sensitivity.

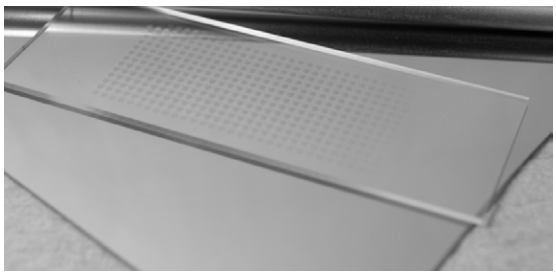

Figure 20. Patterned nanostructured titanium oxide thin film deposited through a hard mask onto a standard microscope glass slide for application in microarray technology.

Carbone *et al* [105] characterized the biocompatibility of nanostructured TiO_2 films produced by the deposition of a supersonic beam of TiOx clusters. The cluster-assembled film supported normal growth and adhesion of primary and cancer cells with no need for coating with extracellular matrix proteins. Physical analysis showed that the films possess a nanoscale granularity and porosity mimicking that of typical extracellular matrix structures and adsorption properties that could allow surface functionalization with different macromolecules such as DNA proteins and peptides. Films of nanostructured titania are proposed as an optimal substrate for different applications in cell-based assays, biosensors, bioactive orthopedic, dental and vascular implants or microfabricated medical devices. Such films may be realized even at a commercial production scale as CBD using a PMCS can be developed into a continuous high-throughput coating technique (figure 20).

7. Conclusions and outlook

The use of beams of clusters and nanoparticles in the gas phase has reached a degree of complexity and maturity that makes this approach very promising for the production of nanostructured materials and systems. The transition from the use of CBD as a tool for basic research to a method for the fabrication of nanostructured systems is driven by the combination of supersonic expansions with aerodynamic

focusing. A careful control on the aerodynamic conditions during cluster production, extraction and deposition is of fundamental importance to meet the requisites necessary for applications: high intensity, stability, repeatability, high lateral resolution and parallel processing.

The cluster beam approach is inherently compatible with planar technologies typical of thin film deposition and it should be further developed in order to improve the compatibility with silicon-based microfabrication technologies. The achievement of this goal will assure CBD a pivotal position in the efforts towards the merging of nanofabrication with microfabrication.

Acknowledgments

We thank G Bongiorno for his help in the preparation of the manuscript.

References

[1] Ulrich G D 1984 *Chem. Eng. News* **62** 22–9
[2] Stark W J and Pratsinis S E 2002 *Powder Technol.* **126** 103–8
[3] Donnet J-B, Bansal R C and Wang M-J (ed) 1993 *Carbon Black* (New York: Dekker)
[4] Braun J H, Baidins A and Marganski R E 1997 *Prog. Org. Coat.* **20** 105–38
[5] Diebold U 2003 *Surf. Sci. Rep.* **48** 53–229
[6] Nalwa H S (ed) 2004 *Encyclopedia of Nanoscience and Nanotechnology* (Stevenson Ranch, CA: American Scientific Publishers)
[7] Roco M 2005 *J. Nanopart. Res.* **7** 707–12
[8] Clavin R K, Zhirnov V V, Bourianoff G I, Hutchby J A, Herr D J C, Hosack H H, Joyner W H and Wooldridge T A 2005 *J. Nanopart. Res.* **7** 573–86
[9] Siegel R W, Hu E and Roco M C (ed) 1999 *Nanostructure Science and Technology: A Worldwide Study* (Loyola College, Maryland: National Science and Technology Council (NSTC)) available from: http://www.wtec.org/loyola/nano/final/
[10] Wegner K and Pratsinis S E 2003 *Chem. Eng. Sci.* **58** 4581–9
[11] Kammler H K, Mädler L and Pratsinis S E 2001 *Chem. Eng. Technol.* **24** 583–96
[12] Singh Y, Javier J R N, Ehrman S H, Magnusson M H and Deppert K 2002 *J. Aerosol Sci.* **33** 1309–25
[13] Wegner K and Pratsinis S E 2003 *AIChE J.* **49** 1667–75
[14] Nakaso K, Shimada M, Okuyama K and Deppert K 2002 *J. Aerosol. Sci.* **33** 1061–74
[15] Nanda K K, Kruis F E, Fissan H and Acet H 2002 *J. Appl. Phys.* **91** 2315–21
[16] Karlsson M N A, Deppert K, Magnusson M H, Karlsson L S and Malm J-O 2004 *Aerosol Sci. Technol.* **38** 948–54
[17] Ostraat M L, De Blauwe J W, Green M L, Bell L D, Atwater H A and Flagan R C 2001 *J. Electrochem. Soc.* **148** G265–70
[18] Krinke T J, Deppert K, Magnusson M H and Fissan H 2002 *Part. Part. Syst. Charact.* **19** 321–6
[19] Krinke T J, Fissan H, Deppert K, Magnusson M H and Samuelson L 2001 *Appl. Phys. Lett.* **78** 3708–10
[20] Milani P and Iannotta S 1999 *Cluster Beam Synthesis of Nanostructured Materials* (Berlin: Springer)
[21] de Heer W A 1993 *Rev. Mod. Phys.* **65** 611–76
[22] Milani P, Piseri P, Barborini E, Podestà A and Lenardi C 2001 *J. Vac. Sci. Technol.* A **19** 2025–33
[23] Mazza T *et al* 2005 *Appl. Phys. Lett.* **87** 103108
[24] Piseri P, Vahedi Tafreshi H and Milani P 2004 *Curr. Opin. Solid State Mater. Sci.* **8** 195–202
[25] Wang X, Kruis, F E and McMurry P H 2005 *Aerosol Sci. Technol.* **39** 611–23
[26] Liu P, Ziemann P J, Kittelson D B and McMurry P H 1995 *Aerosol Sci. Technol.* **22** 293–313
[27] Liu P, Ziemann P J, Kittelson D B and McMurry P H 1995 *Aerosol Sci. Technol.* **22** 314–24
[28] Friedlander S K 2000 *Smoke, Dust and Haze* (New York: Oxford University Press)
[29] Hagena O F and Obert W 1972 *J. Chem. Phys.* **56** 1793–802
[30] Siegel R W 1991 *Annu. Rev. Mater. Sci.* **21** 559–78
[31] Girshick S L, Chiu C P, Muno R, Wu Y U, Yang L, Singh S K and McMurry P H 1993 *J. Aerosol Sci.* **24** 367–82
[32] Pratsinis S E 1998 *Prog. Energy Combust. Sci.* **24** 197–219
[33] Bandyopadhyaya R, Lall A A and Friedlander S K 2004 *Powder Technol.* **139** 193–9
[34] Flagan R C and Lunden M M 1995 *Mater. Sci. Eng.* A **204** 113–24
[35] Granqvist C G and Buhrman R A 1976 *J. Appl. Phys.* **47** 2200–19
[36] Pratsinis S E, Wang G, Panda S, Guiton T and Weimer A 1995 *J. Mater. Res.* **10** 512–20
[37] Ulrich G D 1971 *Combust. Sci. Technol.* **4** 47–57
[38] Wegner K, Walker B, Tsantilis S and Pratsinis S E 2002 *Chem. Eng. Sci.* **57** 1753–62
[39] Landgrebe J D and Pratsinis S E 1990 *J. Colloid Interface Sci.* **139** 63–86
[40] Xiong Y and Pratsinis S E 1993 *J. Aerosol Sci.* **24** 283–300
[41] Fuchs N A and Sutugin A G 1971 *Topics in Current Aerosol Research* ed G M Hidy and J R Brock (New York: Pergamon)
[42] Okuyama K, Kousaka Y, Tohge N, Yamamoto S, Wu J J, Flagan R C and Seinfeld J H 1986 *AIChE J.* **32** 2010–19
[43] Bowles R S, Park S B and Andres R P 1983 *J. Mol. Catal.* **20** 279–87
[44] Buffat P and Borel J P 1976 *Phys. Rev.* A **13** 2287–98
[45] Wu M K, Windeler R S, Steiner C K R, Börs T and Friedlander S K 1993 *Aerosol Sci. Technol.* **19** 527–48
[46] Xing Y and Rosner D E 1999 *J. Nanopart. Res.* **1** 277–91
[47] Tsantilis S, Briesen H and Pratsinis S E 2001 *Aerosol Sci. Technol.* **34** 237–46
[48] Kruis F E, Maisels A and Fissan H 2000 *AIChE J.* **46** 1735–42
[49] Pratsinis S E 1988 *J. Colloid Interface Sci.* **124** 416–27
[50] Hounslow M J, Ryall R L and Marshall V R 1988 *AIChE J.* **34** 1821–32
[51] Tsantilis S and Pratsinis S E 2004 *Langmuir* **20** 5933–9
[52] Wegner K, Stark W J and Pratsinis S E 2002 *Mater. Lett.* **55** 318–21
[53] Ramsey N F 1955 *Molecular Beams* (Oxford: Oxford University Press)
[54] Hagena O F 1974 *Molecular Beams and Low Density Gas Dynamics* ed P P Wegener (New York: Dekker)
[55] Beijering H and Verster N 1981 *Physica* C **11** 327–52
[56] Piseri P, Podestà A, Barborini E and Milani P 2001 *Rev. Sci. Instrum.* **72** 2261–7
[57] 1946 *Oxford Report* #36 UKAEA, Harwell, BR 694, p 2
[58] Becker E W and Bier K 1954 *Z. Naturf.* **9** a 975–86
[59] Becker E W 1979 *Top. Appl. Phys.* **35** 245–68
[60] Ude S and Fernández de la Mora 2003 *J. Aerosol Sci.* **34** 1245–66
[61] Reis V H and Fenn J B 1963 *J. Chem. Phys.* **39** 3240–50
[62] Waterman P C and Stern S A 1959 *J. Chem. Phys.* **31** 405–19
[63] Murphy W K and Sears G W 1964 *J. Appl. Phys.* **85** 1986–7
[64] Israel G W and Friedlander S K 1967 *J. Colloid Interface Sci.* **24** 330–7
[65] Dahneke B E and Flachsbart H 1972 *J. Aerosol Sci.* **3** 345–9
[66] Fernández de la Mora J and Riesco-Chueca P 1988 *J. Fluid Mech.* **195** 1–21
[67] Fernández de la Mora J and Rosell-Llompart J 1989 *J. Chem. Phys.* **91** 2603–15
[68] Fuerstenau S, Gomez A and Fernández de la Mora J 1994 *J. Aerosol Sci.* **25** 165–73
[69] Mallina R V, Wexler A S and Johnston M V 1999 *J. Aerosol Sci.* **30** 719–38
[70] Goo J 2002 *J. Aerosol Sci.* **33** 1493–507

[71] Lee J W, Yi M Y and Lee S M 2003 *J. Aerosol Sci.* **34** 211–24
[72] Zhang X F, Smith K A, Worsnop D R, Jimenez J, Jayne J T and Kolb C E 2002 *Aerosol Sci. Technol.* **36** 617–31
[73] Vahedi Tafreshi H, Benedek G, Piseri P, Vinati S, Barborini E and Milani P 2001 *Eur. Phys. J. Appl. Phys.* **16** 149–56
[74] Vahedi Tafreshi H, Benedek G, Piseri P, Vinati S, Barborini E and Milani P 2002 *Aerosol Sci. Technol.* **36** 593–606
[75] Vahedi Tafreshi H, Piseri P, Barborini E, Benedek G and Milani P 2002 *J. Nanopart. Res.* **4** 511–24
[76] Middha P and Wexler AS 2003 *Aerosol Sci. Technol.* **37** 907–15
[77] Mallina R V, Wexler A S, Rhoads K P and Johnston M V 2000 *Aerosol Sci. Technol.* **33** 87–104
[78] Fernández de la Mora J 1996 *Chem. Eng. Commun.* **151** 101–24
[79] Gentry W R 1988 *Atomic and Molecular Beam Methods* ed G Scoles (Oxford: Oxford University Press)
[80] Bansmann J *et al* 2005 *Surf. Sci. Rep.* **56** 189–275
[81] Ross K J and Sonntag B 1995 *Rev. Sci. Instrum.* **66** 4409–33
[82] Sattler K, Muehlbach J and Recknagel E 1980 *Phys. Rev. Lett.* **45** 821–4
[83] Gatz P and Hagena O F 1995 *Appl. Surf. Sci.* **91** 169–74
[84] Raizer Y P 1991 *Gas Discharge Physics* (Berlin: Springer)
[85] Lieberman M A and Lichtemberg A J 1994 *Principles of Plasma Discharges and Materials Processing* (New York: Wiley)
[86] Haberland H, Karrais M, Mall M and Thurner Y 1992 *J. Vac. Sci. Technol.* A **10** 3266–71
[87] Haberland H, Mall M, Moseler M, Qiang Y, Reiners T and Thurner Y 1994 *J. Vac. Sci. Technol.* A **12** 2925–30
[88] Hihara T and Sumiyama K 1998 *J. Appl. Phys.* **84** 5270–6
[89] Yamamuro S, Sumiyama K and Suzuki K 1999 *J. Appl. Phys.* **85** 483–9
[90] Pratontep S, Carroll S J, Xirouchaki C, Streun M and Palmer R E 2005 *Rev. Sci. Instrum.* **76** 045103
[91] Sumiyama K, Hihara T, Peng D L and Katoh R 2005 *Sci. Technol. Adv. Mater.* **6** 18–26
[92] Maruyama S, Anderson L R and Smalley R E 1990 *Rev. Sci. Instrum.* **61** 3686–93
[93] Milani P and deHeer W A 1990 *Rev. Sci. Instrum.* **61** 1835–38
[94] Dietz T G, Duncan M A, Powers D E and Smalley R E 1981 *J. Chem. Phys.* **74** 6511–2
[95] Geusic M E, Morse M D, O'Brien S C and Smalley R E 1985 *Rev. Sci. Instrum.* **56** 2123–30
[96] Woenckhaus J and Becker J A 1994 *Rev. Sci. Instrum.* **65** 2019–22
[97] Heiz U, Vanolli F, Trento L and Schneider W-D 1997 *Rev. Sci. Instrum.* **68** 1986–94
[98] Pellarin M *et al* 1994 *Chem. Phys. Lett.* **224** 338–44
[99] Barborini E, Piseri P and Milani P 1999 *J. Phys. D: Appl. Phys.* **32** L105–9
[100] Vahedi Tafreshi H, Piseri P, Benedek G and Milani P 2006 *J. Nanosci. Nanotechnol.* **6** 1140–9
[101] Bongiorno G *et al* 2005 *J. Nanosci. Nanotechnol.* **5** 1072–80
[102] Bongiorno G *et al* 2005 *Carbon* **43** 1460–9
[103] Diederich L, Barborini E, Piseri P, Podestà A, Milani P, Schneuwly A and Gallay R 1999 *Appl. Phys. Lett.* **75** 2662–4
[104] Bruzzi M, Miglio S, Scaringella M, Bongiorno G, Piseri P, Podestà A and Milani P 2004 *Sensors Actuators* B **100** 173–6
[105] Carbone R *et al* 2006 *Biomaterials.* **27** 3221–9
[106] Ganteför G, Siekmann H R, Lutz H O and Meiwes-Broer K H 1990 *Chem. Phys. Lett.* **165** 293–6
[107] Siekmann H R, Lüder C, Faehrmann J, Lutz H O and Meiwes-Broer K H 1991 *Z. Phys.* D **20** 417–20
[108] Siekmann H R, Holub-Krappe E, Wrenger B, Pettenkofer C and Meiwes-Broer K H 1993 *Z. Phys.* B **90** 201–6
[109] Cha C Y, Ganteför G and Eberhardt W 1992 *Rev. Sci. Instrum.* **63** 5661–6
[110] Barborini E, Piseri P, Podestà A and Milani P 2000 *Appl. Phys. Lett.* **77** 1059–61
[111] Milani P, Piseri P, Barborini E, Lenardi C, Castelnovo C and Podestà A 2001 *Nanostructured Carbon for Advanced Applications (NATO Advanced Study Institute Series II: Mathematics, Physics and Chemistry)* ed G Benedek *et al* (Dordrecht: Kluwer)
[112] Di Fonzo F, Gidwani A, Fan M H, Neumann D, Iordanoglou D I, Heberlein J V R, Tymiak N, Gerberich W W and Rao N P 2000 *Appl. Phys. Lett.* **77** 910–2
[113] Carroll S J, Pratontep S, Streun M, Palmer R E, Hobday S and Smith R 2000 *J. Chem. Phys.* **113** 7723–7
[114] Palmer R E, Pratontep S and Boyen H-G 2003 *Nature Mater.* **2** 443–8
[115] Melinon P, Hannour A, Prevel B, Bardotti L, Bernstein E, Perez A, Gierak J, Bourhis E and Mailly D 2005 *J. Crystal Growth* **275** 317–25
[116] Camata R P, Atwater H A, Vahala K J and Flagan R C 1996 *Appl. Phys. Lett.* **68** 3162–4
[117] Jacobs H O and Whitesides G M 2001 *Science* **291** 1763–6
[118] Krinke T J, Deppert K, Magnusson M H, Schmidt F and Fissan H 2002 *J. Aerosol Sci.* **33** 1341–59
[119] Ehbrecht M, Kohn B, Huisken F, Laguna M A and Paillard V 1997 *Phys. Rev.* B **56** 6958–64
[120] Ehbrecht M, Ferkel H and Huisken F 1997 *Z. Phys.* D **40** 88–92
[121] Laguna M A, Paillard V, Kohn B, Ehbrecht M, Huisken F, Ledoux G, Papoular R and Hofmeister H 1999 *J. Lumin.* **80** 223–8
[122] Huisken F, Kohn B and Paillard V 1999 *Appl. Phys. Lett.* **74** 3776–8
[123] Huisken F, Ledoux G, Guillois O and Reynaud C 2002 *Adv. Mater.* **14** 1861–5
[124] Voigt F, Brüggemann R, Unold T, Huisken F and Bauer G H 2005 *Mater. Sci. Eng.* C **25** 584–9
[125] Ducati C, Barborini E, Piseri P, Milani P and Robertson J 2002 *J. Appl. Phys.* **92** 5482–9
[126] Bongiorno G, Podestà A, Ravagnan L, Piseri P, Milani P, Lenardi C, Miglio S, Bruzzi M and Ducati C 2006 *J. Mater. Sci.: Mater. Electron.* **17** 427–41
[127] Masenelli B *et al* 2005 *Eur. Phys. J.* D **34** 139–43
[128] Kreibig U and Vollmer M 1995 *Optical Properties of Metal Clusters* (Berlin: Springer)
[129] Gaudry M, Lerme J, Cottancin E, Pellarin M, Vialle J L, Broyer M, Prevel B, Treilleux M and Melinon P 2001 *Phys. Rev.* B **64** 085407
[130] Gaudry M *et al* 2003 *Phys. Rev.* B **67** 155409
[131] Celep G *et al* 2004 *Phys. Rev.* B **70** 165409
[132] Whangbo S W, Jang H K, Kim S G, Cho M H, Jeong K and Whang C N 2000 *J. Korean Phys. Soc.* **37** 456–60
[133] Zhao Z W, Tay B K, Chen J S, Hu J F, Sun X W and Tan S T 2005 *Appl. Phys. Lett.* **87** 251912
[134] Kizaki Y, Osada H and Aoki H 1993 *Japan. J. Appl. Phys.* **32** 5778–90
[135] Peng D L, Sumiyama K, Nozawa N, Hihara T and Morikawa H 2005 *IEEE Trans.Magnetics* **41** 3406–8
[136] Binns C *et al* 2005 *J. Phys. D: Appl. Phys.* **38** R357–79
[137] Qui J-M, Xu Y-H, Judy J H and Wang J-P 2005 *J. Appl. Phys.* **97** 10P704
[138] Kennedy M K, Kruis F E, Fissan H, Mehta B R, Stappert S and Dumpich G 2003 *J. Appl. Phys.* **93** 551–60
[139] Mädler L, Roessler A, Pratsinis S E, Sahm T, Gurlo A, Barsan N and Weimar U 2006 *Sensors Actuators* B **114** 283–95
[140] Kennedy M K, Kruis F E, Fissan H, Nienhaus H, Lorke A and Metzger T H 2005 *Sensors Actuators* B **108** 62–9
[141] Abbet S, Judai K, Klinger L and Heiz U 2002 *Pure Appl. Chem.* **74** 1527–35
[142] Aizawa M, Lee S and Anderson S L 2003 *Surf. Sci.* **542** 253–75
[143] Cadete Santos Aires F J, Sautet P, Rousset J-L, Fuchs G and Mélion P 1994 *J. Vacuum. Sci. Technol.* B **12** 1776–9

[144] Rousset J L, Cadete Santos Aires F J, Bornette F, Cattenot M, Pellarin M, Stievano L and Renouprez A J 2000 *Appl. Surf. Sci.* **164** 163–8
[145] Takeuchi M, Dohshi S, Eura T and Anpo M 2003 *J.Phys. Chem.* B **107** 14278–82
[146] Takeuchi M, Tsujimaru K, Sakamoto K, Matsuoka M, Yamashita H and Anpo M 2003 *Res. Chem. Intermediates* **29** 619–29
[147] Zhou J, Takeuchi M, Zhao X S, Ray A K and Anpo M 2006 *Catal. Lett.* **106** 67–70
[148] Collins J A, Xirouchaki C, Palmer R E, Heath J K and Jones C H 2004 *Appl. Surf. Sci.* **226** 197–208
[149] Gidwani A 2003 *PhD Thesis* Department of Mechanical Engineering, University of Minnesota, Minneapolis 55455, USA